

CAN COAL SCIENCE BE PREDICTIVE

Peter R. Solomon, David G. Hamblen, Michael A. Serio, Zhen-Zhong Yu, and Sylvie Charpenay
Advanced Fuel Research Inc., 87 Church Street, East Hartford, CT 06108

KEY WORDS: Coal, Pyrolysis, Network

ABSTRACT

This paper considers the development of a predictive macromolecular network decomposition model for coal conversion which is based on experimental results from a variety of modern analytical techniques. Six concepts which are the foundation of the Functional Group, Depolymerization, Vaporization, Crosslinking (FG-DVC) model are considered: 1) The decomposition of functional group sources in the coal yield the light gas species in thermal decomposition. The amount and evolution kinetics can be measured by TG-FTIR, the functional group changes by FT-IR and NMR. 2) The decomposition of a macromolecular network yields tar and metaplast. The amount and kinetics of the tar evolution can be measured by TG-FTIR and the molecular weight by FIMS. The kinetics of metaplast formation and destruction can be measured by solvent extraction, by Geissler plastometer and by proton magnetic resonance thermal analysis (PMRTA). 3) The molecular weight distribution of the metaplast depends on the network coordination number (average number of attachments on aromatic ring clusters). The coordination number can be determined by solvent swelling and NMR. 4) The network decomposition is controlled by bridge breaking. The number of bridges broken is limited by the available donatable hydrogen. 5) The network solidification is controlled by crosslinking. The changing crosslink density can be measured by solvent swelling and NMR. Crosslinking appears to occur with evolution of both CO_2 (prior to bridge breaking) and CH_4 after bridge breaking. Thus, low rank coals (which form a lot of CO_2) crosslink prior to bridge breaking and are thus thermosetting. High volatile bituminous coals (which form little CO_2) undergo significant bridge breaking prior to crosslinking and become highly fluid. Weathering, which increases the CO_2 yield, causes increased crosslinking and lowers fluidity. 6) The evolution of tar is controlled by mass transport in which the tar molecules evaporate into the light gas species and are carried out of the coal at rates proportion to their vapor pressure and the volume of light gases. High pressures reduce the volume of light gases and hence reduces the yield of heavy molecules with low vapor pressures. These changes can be studied with FIMS.

The paper describes how the coal kinetic and composition parameters are obtained by TG-FTIR, solvent swelling, solvent extraction, and Geissler plastometer data. The model is compared to a variety of experimental data in which heating rate, temperature, and pressure are all varied. There is good agreement with theory for most of the data available from our laboratory and in the literature.

INTRODUCTION

The question addressed by this paper is, can coal science be predictive? More specifically, is it possible, to accurately predict the way a coal behaves in a coal conversion process, given coal characteristics which can be measured in the laboratory. For example, Fig. 1 illustrates the behavior of coal in combustion. The left hand side of the figure shows a picture of a coal burning in a reactor where the coal is injected into the center of a hot air stream. The processes that occur are illustrated on the right hand side. Starting from the bottom, the figure represents the heating of the coal, coal softening, devolatilization, swelling, the ignition of the volatiles, the formation of soot, the burning of the volatiles, the ignition of the char, the combustion of the char, and finally the fragmentation of the char which determine the ultimate distribution of the ash particles. Can one qualitatively predict pyrolysis yields, swelling, soot formation, char reactivity, etc.?

As a second example, consider coal in a liquefaction process. The important step is the fragmentation of the coal macromolecule into small pieces. As shown in Fig. 2, that fragmentation takes place very quickly for a bituminous coal. The coal dissolves into the solvent, and the subsequent reactions between the solvent and the coal are all liquid-liquid phase interactions, which can occur very rapidly. In a lignite, this fragmentation process is prevented by low temperature crosslinking. The result is that

CAN COAL SCIENCE BE PREDICTIVE

Peter R. Solomon, David G. Hamblen, Michael A. Serio, Zhen-Zhong Yu, and Sylvie Charpenay
Advanced Fuel Research Inc., 87 Church Street, East Hartford, CT 06108

KEY WORDS: Coal, Pyrolysis, Network

ABSTRACT

This paper considers the development of a predictive macromolecular network decomposition model for coal conversion which is based on experimental results from a variety of modern analytical techniques. Six concepts which are the foundation of the Functional Group, Depolymerization, Vaporization, Crosslinking (FG-DVC) model are considered: 1) The decomposition of functional group sources in the coal yield the light gas species in thermal decomposition. The amount and evolution kinetics can be measured by TG-FTIR, the functional group changes by FT-IR and NMR. 2) The decomposition of a macromolecular network yields tar and metaplast. The amount and kinetics of the tar evolution can be measured by TG-FTIR and the molecular weight by FIMS. The kinetics of metaplast formation and destruction can be measured by solvent extraction, by Geissler plastometer and by proton magnetic resonance thermal analysis (PMRTA). 3) The molecular weight distribution of the metaplast depends on the network coordination number (average number of attachments on aromatic ring clusters). The coordination number can be determined by solvent swelling and NMR. 4) The network decomposition is controlled by bridge breaking. The number of bridges broken is limited by the available donatable hydrogen. 5) The network solidification is controlled by crosslinking. The changing crosslink density can be measured by solvent swelling and NMR. Crosslinking appears to occur with evolution of both CO_2 (prior to bridge breaking) and CH_4 after bridge breaking. Thus, low rank coals (which form a lot of CO_2) crosslink prior to bridge breaking and are thus thermostetting. High volatile bituminous coals (which form little CO_2) undergo significant bridge breaking prior to crosslinking and become highly fluid. Weathering, which increases the CO_2 yield, causes increased crosslinking and lowers fluidity. 6) The evolution of tar is controlled by mass transport in which the tar molecules evaporate into the light gas species and are carried out of the coal at rates proportion to their vapor pressure and the volume of light gases. High pressures reduce the volume of light gases and hence reduces the yield of heavy molecules with low vapor pressures. These changes can be studied with FIMS.

The paper describes how the coal kinetic and composition parameters are obtained by TG-FTIR, solvent swelling, solvent extraction, and Geissler plastometer data. The model is compared to a variety of experimental data in which heating rate, temperature, and pressure are all varied. There is good agreement with theory for most of the data available from our laboratory and in the literature.

INTRODUCTION

The question addressed by this paper is, can coal science be predictive? More specifically, is it possible, to accurately predict the way a coal behaves in a coal conversion process, given coal characteristics which can be measured in the laboratory. For example, Fig. 1 illustrates the behavior of coal in combustion. The left hand side of the figure shows a picture of a coal burning in a reactor where the coal is injected into the center of a hot air stream. The processes that occur are illustrated on the right hand side. Starting from the bottom, the figure represents the heating of the coal, coal softening, devolatilization, swelling, the ignition of the volatiles, the formation of soot, the burning of the volatiles, the ignition of the char, the combustion of the char, and finally the fragmentation of the char which determine the ultimate distribution of the ash particles. Can one qualitatively predict pyrolysis yields, swelling, soot formation, char reactivity, etc.?

As a second example, consider coal in a liquefaction process. The important step is the fragmentation of the coal macromolecule into small pieces. As shown in Fig. 2, that fragmentation takes place very quickly for a bituminous coal. The coal dissolves into the solvent, and the subsequent reactions between the solvent and the coal are all liquid-liquid phase interactions, which can occur very rapidly. In a lignite, this fragmentation process is prevented by low temperature crosslinking. The result is that

there is no quick solubilization of the coal, and most of the reaction takes place between the solvent and a solid crosslinked residue. Can one predict macromolecular fragmentation and crosslinking?

The research conducted during the last ten years suggests that many of the steps discussed above can be accurately predicted. Figure 3 shows the concept employed in our laboratory for developing predictive capabilities. We start with a set of laboratory characterization procedures that allow the appropriate kinetic and composition parameters for coal to be determined. Five kinds of experiments allow us to define the parameters for our model. The most important is the TG-FTIR, a thermogravimetric (TG) analyzer with the analysis of the evolved product by Fourier Transform Infrared (FT-IR) spectroscopy (1). This instrument allows us to determine the amount of the volatiles, their composition, the kinetics for their evolution, the reactivity of the char, and also the moisture and ash content of the coal. We also measure the solvent swelling ratio (2,3), the extract yield, and the fluidity in a Geissler plastometer (4), and employ nuclear magnetic resonance (NMR) (5), and Field Ionization Mass spectrometry (FIMS) data (6). These experiments determine the macromolecular network parameters for the model.

The model is the FG-DVC model (7,8). The letters FG stand for Functional Group, and DVC for Depolymerization, Vaporization and Crosslinking. The FG model considers certain functional groups in the coal which decompose to form the light gas species (9-12). At the same time, the DVC model describes the overall depolymerization of the macromolecular network which combines bridge breaking and crosslinking to produce fragments of the coal macromolecular (13-15). These fragments are then subjected to transport behavior, specifically the vaporization of the lightest fragments to form tar. The fragmentation process provides a second mechanism for the removal of functional groups from the coal. The model, whose parameters are determined in the laboratory at moderate temperatures and one atmosphere, can then be used to extrapolate away from the laboratory conditions to predict pyrolysis and combustion in high temperature reactions, or liquefaction at high pressure. Recently, we have explored extrapolation of the kinetics and reactions to low temperature geological transformations in coal beds (16).

The model for coal thermal decomposition has six basic concepts:

- Functional Groups (decompose to produce light gases)
- Macromolecular Network (decomposes to produce tar and metaplast)
- Network Coordination Number (determines fragment molecular weights)
- Bridge Breaking (limited by hydrogen availability)
- Crosslinking (related to gas evolution)
- Mass Transport of Tar (evaporation of light network fragments into light gases)

The first concept is that light gases are formed by the decomposition of certain functional groups in the coal. For example, methyl groups can decompose to form methane, carboxyl groups can decompose to form CO₂, etc. (9-12, 17-20). The second concept is that coal consists of a macromolecular network (2,3,7,13-15,21-36). This network is made up of fused aromatic ring clusters (which are described by their molecular weight) linked by bridges, some of which are relatively weak. There are some unattached parts of the network which can be extracted. Sometimes, there is also a second polymethylene component (37-41). When heated, this network decomposes to produce smaller fragments. The lightest of the fragments evaporate to produce tar (7,42), and the heavier fragments form the metaplast. These heavier molecules are the primary liquid fragments in liquefaction or the fragments that make coal fluid (8,43).

The third concept is that one of the most important properties of the network is its coordination number. The coordination number describes the geometry of the network by specifying how many possible attachments there are per aromatic ring cluster (node) (31-36). For example, a linear polymer chain has a coordination number of 2, because each fused aromatic ring has two possible attachments to link it in the chain. On the other hand, a "fish net" has a coordination number of 4, because there are four possible attachments at each node. The coordination number controls the molecular weight distribution of the network fragments at a given extent of decomposition. The extent of decomposition is specified by the probability that the possible attachments are made. For example, for 20% of broken

bridges, a linear chain is totally fragmented, while a "fish net" will have some holes but is almost totally connected. In describing the network, a crosslink is defined to occur at a node where there are more than two attachments. The coordination number is thus, related to the crosslink density. With no possible crosslinks, the coordination number is two. With increasing crosslink density the coordination number increases.

The second important property of the network is the fraction of possible attachments which are actually made. During thermal decomposition, this fraction is determined by the rates of bond breaking and crosslinking (7,15,44-47). The factors which control how many of the weak links can break are the rate constant and the amount of hydrogen that can be donated from the coal to stabilize the free radicals which form when the links break (10).

A competitive process with the bond breaking is the retrogressive process of crosslinking. Crosslinking reactions appear to be related to the evolution of certain gases (7,15,44,47). Specifically, for low rank coals, crosslinking at low temperature (prior to bridge breaking) seems to be related to the evolution of carbon dioxide (or possibly water). For coals of all rank, a higher temperature crosslinking event (following bridge breaking) seems to be related to the evolution of methane. At high temperatures, the evolution of hydrogen is also related to crosslinking.

The final concept is that the tar evolution is controlled by mass transport. Bridge breaking and crosslinking produce fragments with a molecular weight distribution. The lightest fragments can leave the coal melt by evaporation into the light gas species (7,42). The heavier fragments remain, forming the metaplast which controls the coal's fluidity.

The remainder of the paper describes how these concepts are incorporated into a practical predictive model. Section II considers the FG-DVC model in detail. It discusses each of the six concepts and the evidence for each assumption. Section III considers the experiments employed to obtain the model parameters, and Section IV compares predictions of the model with a variety of experimental data. Section V is the summary.

COAL PYROLYSIS MODEL

Functional Group Decomposition Model

Figure 4 illustrates the phenomena in coal thermal decomposition considered in the functional group model. The figure is not meant to describe the exact structure of coal or the exact chemistry which occurs in pyrolysis. It is meant to illustrate the kinds of structures that are being considered and the classes of phenomena that can occur. The important processes are the decomposition of the individual functional group to form the light gases and the competitive decomposition of the macromolecular network to form fragments, the lightest of which can evaporate as tar.

Figure 4a shows a representative piece of a Pittsburgh Seam coal macromolecule. The structure is based on measurements of the aromatic ring cluster size, the functional group composition and the elemental composition (48). The molecule consists of several fused aromatic ring clusters linked by labile bridges. The ring clusters have various functional groups attached to them. When the coal is heated, two things happen to the functional groups. The first is that certain functional groups can decompose to form light gases. The second is that fragmentation of the network, and removal of light fragments as tar, can cause the same type of functional group to be removed as part of the tar. So, there are two parallel processes for the volatilization of the functional groups.

The way the coal behaves during pyrolysis is illustrated in Fig. 4b. The carbon-carbon aliphatic bridge in the upper left hand corner of the molecule (labeled 2) broke and picked up hydrogen to form two methyl groups. This process creates a fragment which is light enough to evolve as tar. There is also independent decomposition of functional groups to form light gases. The carboxyl group that was shown in the middle of Fig. 4a is shown as a carbon dioxide evolving in Fig. 4b. Methyl groups have decomposed to form methane, there has been a condensation of hydroxyl groups to form water and an ether link (labeled 3), mercaptans decompose to form H₂S, etc.

The evidence for this description is as follows: 1) for bituminous coals and low rank coals heated rapidly, the tar is strikingly similar in elemental and functional group composition to the parent coal (9,10,48-50). The tar appears to consist of representative fragments of the parent coal macromolecule; 2) there is a correlation between the decrease in the functional group sources in the char and the evolution of specific gases (9-12); 3) there is a systematic variation in functional group composition with rank, and this variation is correlated with the evolved gas composition.

While there is good evidence for the above description, the details of the chemistry are not yet well understood. Also, tar produced from low rank coals at low heating rates appears to be significantly different in composition from the coal (51) and is probably dominated by polymethylenes.

Macromolecular Network Decomposition Model

The concept of a macromolecular network decomposition model, is illustrated in Fig. 5, which recently appeared in a paper by Grant and coworkers (36). The figure represents aromatic ring clusters with four possible attachments to their neighbors, arranged in a "fish net" type network, (a network with a coordination number of 4). Figure 5a illustrates what happens when 20% of the possible attachments are broken. As can be seen, there are only three fragments which are created, shown by the clusters with boxes around them. The breaking of 20% of the bridges produces very little fragmentation of the network. On the other hand, consider in Fig. 5b what happens when 45% of the bridges are broken. Now, there is a much higher concentration of fragments and the fragments have a molecular weight distribution from monomers up to 7-mers (consisting of 7 fused ring clusters linked together). The lightest of these fragments, monomers, dimers, and trimers can evaporate into the light gas species and are removed from the coal particles as tar. The heavier fragments make up the metaplast. The lightest of these can be extracted using solvent, while others are too heavy to be extracted. The presence of a sufficiently large fraction of these fragments are what makes these materials fluid.

Network Coordination Number

The importance of the network coordination number is illustrated in Figs. 5 and 6. In Fig. 5a with 20% of the bridges broken in a "fish net", only a small number of fragments are produced, and they are all monomers. On the other hand, if 20% of the bridges in the linear chain are broken, 100% of the material becomes fragments and there will be many dimers, trimers, etc. Thus, the molecular weight distribution of the fragments depends very strongly on the coordination number.

In Fig. 5, the molecular distribution was computed using Monte Carlo calculations in which a representative network is set up in computer memory and the fragment molecular weight distribution is calculated after the broken bridges are randomly distributed. Alternatively, a technique called percolation theory allows a closed form analytical solution of the molecular weight distribution as a function of the number of actual attachments per ring cluster.

Figure 6 shows percolation theory calculations for networks with two different coordination numbers: Fig. 6a is for a coordination number of 2.2 and Fig. 6b is for 4.6. The variable σ is one less than the coordination number. The figure shows the calculated distributions of: i) monomers, ii) up to trimers (i.e., monomer, dimer, trimer) representative of what might be evolved as tar for a ring cluster size of 300 Daltons, iii) the yields of all n-mer up to ten representative of extractable material, and 4) the yield of all n-mers. These are plotted as a function of α , which is the average number of bridges per fused aromatic rings. This term α is equal to the probability, p , that a bridge is occupied times the coordination number of the network divided by two, $\alpha = p(\sigma + 1)/2$. As can be seen, there is a very different distribution of fragments depending on the coordination number. For example, at a value of $\alpha = 0.9$, the network with coordination number 4.6 has most of the fragments in the tar, with only a small number of n-mers between 3 and 10 and almost no n-mers above 10. On the other hand, for a network with a coordination number of 2.2 at $\alpha = 0.9$, there is a smaller number of monomers, a somewhat smaller concentration of tar, but a much higher concentration of n-mers up to 10 and a 100% yield of all n-mers. In other words, for 0.9 bridges per cluster, most of the molecules had decomposed to produce fragments of one size or another.

The DVC model was originally implemented using a Monte Carlo solution method, which allows an arbitrary network geometry. Percolation theory, however, offers significant benefits in computational speed and reproducibility, at the cost of restricting the network geometries.

As we shall see below, in the Monte Carlo version of the model, the starting network is represented by linear chains of monomers (6-12 aromatic clusters) with some amount of crosslinking which tie the chains together. Thus the starting network has a coordination number between 2 (straight chains) and three or more (fully cross linked). As pyrolysis proceeds, the linear chain bonds (bridges) are broken, and crosslinks (the side bonds) are formed. Thus, the coordination number, or degree of branching, increases with extent of pyrolysis. The conventional percolation theory models of coal decomposition do not model this feature. With conventional percolation theory, one can make any identification of the various chemical bonds with the percolation lattice bonds, so that the probability of a bond being occupied tracks the chemistry; but the occupied bonds must be randomly distributed within the lattice. The structure cannot be converted from "chain-like" to "fishnet-like".

The DVC model predicts, and experiments confirm, that there are more than one kind of bond (bridges and crosslinks)-which have different coordination numbers, and independent probabilities of being broken. To take advantage of the benefits of percolation theory, we have extended percolation theory on a Bethe lattice (one with no loops) to use two independent sub-networks, as illustrated in Figure 7 (32). In the Figure, double lines represent one of the bond types, while single lines represent the other. As can be seen by comparing Fig 7a and 7b, this lattice has the desired feature of modeling a transition from chain-like structures (a) to fishnet structures (b). The mathematics of this 2-bond percolation theory follows closely that of the standard theory (32). A comparison of the results obtained from the 2-bond percolation theory agree well with those obtained from the original Monte Carlo calculations, as will be discussed in the Results Section.

Bridge Breaking and Hydrogen Utilization

There are two questions with respect to bridge breaking: what is the bridge breaking rate and how many bridges break. Pyrolysis rates have been reviewed by a number of authors (10,52-54). One of the problems in pyrolysis over the last two decades is a very wide variation in the reported rates for either weight loss or tar evolution in pyrolysis.

Figure 8a presents several of the extremes in rates reported prior to 1985 for high heating rate experiments (10,55-58). At 800°C there is almost a four order of magnitude variation in the rate constant which has been reported. An analysis of the data shows that one can not ascribe this sort of variation in kinetics to variations in the coal type, because investigators who measured more than one coal type found that the variations in kinetics rates among coals are typically within a factor of 10. So there has to be another explanation for why there is such a wide variety of reported rates. The answer appears to be the knowledge of the coal particle temperatures (53,54,59-62). Almost none of the experiments are done with direct measurements of the coal particle temperature. For entrained flow reactor experiments, the temperature is usually calculated and the calculations depend critically on the rate of mixing of the preheated gases with the coal stream. A factor of two error in the heating rate can lead to errors of hundreds of degrees celsius in the particle temperature during pyrolysis. For heated grid experiments, temperature measurements are made with a thermocouple and the inference is made that the thermocouple temperature is the same as the coal particle temperature. Recent reviews of experiments for Pittsburgh Seam coal heated at 1000°C/sec show a wide variation in pyrolysis temperatures, suggesting that this is just not a good assumption (60,63).

Since 1985, several experiments have been performed in which coal particle temperatures were measured during pyrolysis (12,53,61,62,64). Careful experiments have also been performed at several low heating rates where the thermocouple temperature is a good measure of the coal particle temperature (65,66). As can be seen from Fig. 8b, the data are much more tightly grouped. There is a systematic variation with the rank of the coal and the kinetic rate constants appear to have an activation energy between 45 and 55 Kcal. This is the magnitude one would expect for the kind of labile bridges depicted in Fig. 4 (14,67).

Besides the kinetic rate for bridge breaking, one needs to know the number of bridges that can be broken. The number depends upon the amount of hydrogen that is available to stabilize the free radicals formed when bridges break. How the hydrogen utilization controls the amount of tar and its hydrogen concentration is illustrated in Fig. 9. The figure is based on the following consideration: every time a bridge is broken, the available hydrogen is used to stabilize the free radicals. Two radicals are assumed to be stabilized per tar molecule. If the tar is made up of large fragments, the utilization of hydrogen per unit weight of tar is very efficient. On the other hand, if the tar consists of small molecules, the utilization of hydrogen is much less efficient. The figure shows the results for 0.3% hydrogen in the coal available for donation to the tar. The figure presents the yield of tar and the percent of additional hydrogen in the tar as a function of the average molecular weight in the tar. For an average molecular weight of 100 Daltons, 15% tar is produced. The amount of additional hydrogen in the tar is 2%. On the other hand, at an average molecular weight of 300 Daltons the yield is up to 45%, while the weight percent of additional hydrogen per unit mass is only 0.7%. The average molecular weight of the tar is affected by crosslinking, pressure, heating rate, and bed geometry.

Crosslinking

During pyrolysis, another important process occurs besides bridge breaking. It is the process of crosslinking, where new bonds are formed between the fused aromatic ring clusters. One of the ways of measuring the crosslink density is through solvent swelling (2,3), in which a solvent (e.g., pyridine) is used to swell the char or coal (7,15,44-47). To understand how solvent swelling indicates the crosslink density, consider the analogy of an air mattress. An air mattress is stitched in long rows along the length of the mattress. When the mattress is inflated there are several connected small tubes, instead of one big round tube. The small tubes have a smaller volume than one large tube and the volume can be used to infer the limiting circumference of the tubes. In a similar manner, the addition of the solvent to a coal indicates the circumference of linked molecules that make a loop to limit the swelling. Since it is crosslinks (more than two attachments per cluster) that allow loops to be formed, the amount of swelling indicates the average molecular weight between crosslinks.

Figure 10 shows the behavior of the solvent swelling ratio as a function of the char temperature for coals of several ranks. Chars are produced by heating up to the indicated temperatures at 30°C/min in an inert atmosphere and then cooling. These chars are subjected to solvent swelling experiments which determines the volume of swollen coal divided by the unswollen volume. Coals have solvent swelling ratios as high as 2.7. As char is formed, new crosslinks reduce the swelling ratio to unity. The solvent swelling ratio in Fig. 10 is normalized. The parameter x is the difference in solvent swelling ratio between the coal and the char divided by the maximum differences that can be achieved. This normalization allows us to compare different coals with different starting solvent swelling ratios in a convenient manner. Figure 10 presents $1 - x$ as a function of the char temperature. If $x = 0$, we have a material that swells the same as coal and if $x = 1$ we have a fully crosslinked char.

There is a wide variation in behavior depending upon rank. This rank dependence of the crosslinking behavior was first noted by Suuberg and coworkers (44) who measured a lignite and a bituminous coal and found the same sort of difference that has been exhibited here. The lowest rank coal, Zap lignite, is shown by the open squares. At temperatures as low as 200°C, the char starts to undergo crosslinking, loosing most of its solvent swelling properties by a temperature of 400°C. It is between 400 and 500°C that most of the pyrolysis weight loss is occurring for this material. Thus, for a low rank coal, the crosslinking occurs well in advance of the bridge breaking.

For higher rank coals, the crosslinking event is delayed relative to bridge breaking. For a highly softening bituminous coal like Pittsburgh Seam coal, or Kentucky No. 9, we find the material swells even more as it is heated into the region of pyrolysis, and only looses its solvent swelling properties after most of the weight loss has occurred in pyrolysis. There is, thus, a very strong rank dependence of the crosslinking behavior. Low rank coals crosslink early, prior to bridge breaking, while high rank coals undergo crosslinking after most of the bridge breaking has taken place.

The results of solvent swelling experiments are not unambiguous because the solvent swelling ratio depends on two things: 1) the crosslink density and 2) the solvent interaction parameter. This

parameter can change with the functional group composition of the coal. Since the functional group composition will change as the coal pyrolyzes, the change in solvent swelling ratio could be due to the change in the functional group composition, not crosslinking. However, an analysis of how much the solvent swelling ratio may change with the functional group composition indicates that the kind of drastic change from a solvent swelling ratio of 2.7, typical for coal, down to 1 for char is not likely to occur for the small changes in the functional group composition with low temperature pyrolysis (47).

Another way of investigating the crosslink density is by experiments done using nuclear magnetic resonance (NMR). The work was performed at the University of Utah in collaboration with Solum and coworkers (68). Results of the NMR experiments are shown in Fig. 11. The NMR experiments employ cross polarization with magic angle spinning and dipolar dephasing (5). Dipolar dephasing allows the determination of the functional group form of the carbons that are being studied. When all the different kinds of bonds are considered, it is possible to determine an average molecular weight for the ring clusters and also the average number of attachments per ring cluster. In Fig. 11, the average number of attachments are compared to the solvent swelling data for Pittsburgh Seam bituminous coal and a North Dakota lignite. The average number of attachments determined by the NMR are also normalized to determine an NMR index which can be compared to $1 - x$. Figure 11a compares the results for the lignite. The change in crosslink density determined by NMR is in reasonable agreement with that determined by the solvent swelling ratio. As can be seen, the material starts to crosslink at a reasonably low temperature and is almost completely crosslinked by a temperature of about 700 K (427°C), prior to significant bond breaking. For the Pittsburgh Seam coal shown in Fig. 11b the NMR index is in reasonable agreement with the solvent swelling ratio, and in this case both indices show that the char has not undergone appreciable crosslinking by a temperature of 700.

To develop an understanding of the chemistry of crosslinking, we attempted to determine whether the addition of crosslinks could be correlated with any other observation, specifically, the evolution of gases. In the initial work of Suuberg and coworkers (44), they noted that the one gas species which correlated with the early creation of crosslinking in the lignite was carbon dioxide.

Figure 12 shows the results obtained in our laboratory. Figure 12a presents the parameter x as a function of the carbon dioxide yield divided by 44 so that it is on a molecular basis. In Fig. 12 we have plotted x rather than $1 - x$ which was plotted in Figs. 10 and 11. For a wide variety of experiments (some at high heating rates and some at low heating rates) there is a very reasonable correlation between the loss of swelling and the appearance of carbon dioxide in pyrolysis. For all the low rank coals studied, there appears to be a good correlation between the appearance of crosslinks and the appearance of carbon dioxide. The line shown in Fig. 12a is from our FG-DVC model, where one crosslink is assumed for each carbon dioxide evolved.

For a higher rank coal, which does not produce significant yields of CO_2 , a different correlation is observed. Figure 12b compares the normalized solvent swelling ratio for a Pittsburgh Seam coal with the evolution of methane divided by 16. There is a good correlation between these two parameters for chars created at a number of different temperatures at high heating rates. The line in Fig. 12b is from the FG-DVC model, where it is assumed that one crosslink is formed for each methane evolved.

We examined the correlation of the loss of swelling with other parameters and found the correlation between carbon dioxide and methane to be the best. There is a correlation for low rank coals between the formation of crosslinks and the water evolution, but not quite as good as for CO_2 . There was no good correlation for high rank coals between crosslinking and tar evolution.

Three experiments which exhibit the phenomena of bridge breaking and crosslinking are presented in Fig. 13. Figure 13a presents the proton magnetic resonance thermal analysis (PMRTA) experiment done at CSIRO by Lynch, Sakurovs and coworkers (69-71). This experiment, which measures the relaxation time for protons, can distinguish between protons attached to mobile molecules (which are free to rotate) and those attached to a rigid lattice. The higher the concentration of mobile protons, the lower the values of the parameter M_{2T} . The data taken at 4°C/sec was provided by Dr. Sakurovs (72). The decrease in M_{2T} at low temperatures appears to be associated with melting, the sharp drop

in M_{2T} above 400°C is due to bridge breaking and the sharp increase of M_{2T} above 440°C is due to the crosslinking.

Figure 13b shows fluidity data measured with a Geissler plastometer for the same coal at a similar heating rate (3°C/sec) (4). While the fluidity below 400°C is probably due to melting, above 400°C bond breaking becomes important, while above 440°C crosslinking resolidifies the network.

Figure 13c presents data of Fong (73) on the extract yield in chars produced at a high heating rate of 640°C/sec. The maximum extract yield occurs at a much higher temperature than for the other two experiments due to the high heating rate. The increase in extract yield is due to bridge breaking and the decrease to crosslinking.

Transport

The above discussion shows how bridge breaking and crosslinking, can fragment the macromolecular network and allow small pieces to be formed. The evolution of tar is controlled by the formation of these small fragments and their transport out of the metaplast. In our FG-DVC model, we've assumed a very simple transport process. The assumption is that the fragments reach their equilibrium vapor pressure in the light gas species and are removed from the metaplast by convective transport in the light gas species (7). In a highly fluid coal, the expulsion of the light gases occurs by bubble transport. In a low rank thermosetting coal the transport of the light gas species is through the pores. In either case, the degree to which the tar molecules are transported depends upon the volume of light species that evolve and the vapor pressure of the molecule. The low macromolecular weight species that have high vapor pressure are therefore easily transported while heavy molecular weight species are not. The result is that the tar for a bituminous coal pyrolyzed at 1 atmosphere or below consists of molecules up to about 800 Daltons. As the pressure is increased the volume of the light gases is reduced and those marginal heavy products, which were previously transported at one atmosphere, can no longer be transported. Thus, as pressure is increased, the average molecular weight of the tar is reduced. The amount of tar is also reduced because of the reduced efficiency of hydrogen utilization.

For low rank coals, low temperature crosslinking increases the effective coordination number of the network and only small molecules are produced. The yields are low and pressure has little influence on the yield or molecular weight distribution.

Summary of FG-DVC Model

Figure 14 summarizes the FG-DVC model. In Fig. 14a we start with an assumed macromolecular network. In the Monte Carlo version of the model, each piece of this network is actually described in the computer memory. The description of the network contains the molecular weight of the aromatic ring clusters (shown as the number in the circles), and the crosslinking density (shown by the vertical double line). The potential number of labile bridges (related to the donatable hydrogen) are indicated by the single horizontal lines. The starting molecule is constructed from linear chains of a certain length (typically between 6 and 12 aromatic ring clusters) connected by the appropriate number of crosslinks. When this is done a certain number of the chains may be unattached to the rest of the macromolecular network. These are the guest molecules whose molecular weight is less than 3000 Daltons and would be pyridine soluble. The length of the chains is adjusted to obtain the proper pyridine solubles. The number of crosslinks is picked to get a coordination number which yields the right ratio of tar to heavier fragments (e.g., extracts) in the metaplast. The number of labile bridges (amount of donatable hydrogen) is picked to get the proper tar yield in the TG-FTIR experiments.

Figure 14b considers what happens during pyrolysis. As the temperature increases, some of the weak bridges (which are the single horizontal lines), can break according to the bridge breaking rate. The hydrogen limitation is accomplished by requiring that for each bridge that is broken, another one of the labile bridges becomes an unbreakable bridge as its hydrogen is used to stabilize the free radicals caused by the broken bridges. Thus, for each broken bridge, two of the labile bridges are consumed. The broken bridges and new unbreakable bridges are distributed randomly.

In the model, the crosslinking is assumed to correlate with the CO₂ and methane evolution. The evolution of these species is determined from the functional group part of the model and one crosslink is inserted randomly for each carbon dioxide and each methane group which is evolved. If bridge breaking dominates over crosslinking, the macromolecular network is broken up into smaller fragments. On the right hand side of the figure, the molecular weight distribution which results from the bridge breaking and crosslinking events is shown. Molecules below 3000 Daltons are increased, the lightest molecules escape as tar, and the rest of the network is described as pyridine insoluble.

Figure 14c shows the network at the conclusion of the pyrolysis process. When all the labile bridges are consumed, the decomposition of the network is complete. All of the network is completely connected by unbreakable bridges, and is highly crosslinking. All the previously loose fragments have been incorporated into the network by crosslinking or have escaped as tar.

ANALYSIS OF COMPOSITION AND KINETIC PARAMETERS

In this section, the laboratory characterization to determine the model parameters is considered. An analysis by TG-FTIR is employed to determine kinetic rates and functional group compositions. Solvent swelling, solvent extraction, and fluidity measurements in a Geissler plastometer are employed to obtain information on the molecular weight distribution of the metaplast and hence determine the network parameters. NMR and FIMS are used to determine the molecular weight of the ring clusters. These measurements are considered below.

TG-FTIR

Apparatus - As indicated in Fig. 3, TG-FTIR analysis of coal is employed to obtain the composition and kinetic parameter for the model. A schematic of the instrument is presented in Fig. 15. Its components are as follows: a DuPont™ 951 TGA; a hardware interface (including a furnace power supply); an Infrared Analysis 16 pass gas cell with transfer optics; a MICHELSON MB Series FT-IR; (Resolution: 4 cm⁻¹, Detector: MCT); and a PC-AT compatible computer. The cell is connected without restrictions to the sample area and a helium sweep gas is employed to bring evolved products from the TGA directly into the gas cell. This instrument is now available as the TG/plus from Bomem, Inc.

The most difficult volatiles to analyze are the tars which condense at room temperature. In the TG/plus, the rapid cooling from the high thermal conductivity helium sweep gas causes these products to form an aerosol which is fine enough to follow the gas through the analysis cell. The aerosol is also fine enough that there is little scattering of the infrared beam and it thus appears as though the tar was in the gas phase.

As an example of the analysis procedure, the pyrolysis and oxidation of a bituminous coal is described. More detail can be found in Ref. 1. Figure 16a illustrates the weight loss from this sample and the temperature history. A 25 mg sample of Pittsburgh Seam coal, loaded in the sample basket of the DuPont™ 951, is taken on a 30°C/min temperature excursion in the helium sweep gas, first to 150°C to dry, then to 900°C for pyrolysis. After cooling, a small flow of O₂ is added to the furnace at the 57 minute mark and the temperature is ramped to 900°C for oxidation.

During this excursion, infrared spectra are obtained once every forty seconds. As discussed previously (1) the spectra show absorption bands for CO, CO₂, CH₄, H₂O, SO₂, COS, C₂H₄, HCl, and NH₃. The spectra above 400°C also show aliphatic, aromatic, hydroxyl, carbonyl and ether bands from tar. The evolution of gases derived from the IR absorbance spectra are obtained by a quantitative analysis program which employs a database of calibration spectra for different compounds. The routine decides which regions of each calibration spectrum to use for best quantitation with the least interferences. A correlation between the sample spectrum and the reference spectrum is performed to determine gas amounts. A database of integration windows is also available for tracking functional groups absorptions. Tar quantitation is discussed in Ref. 1. The routine is fast enough so that the product analysis can be performed and displayed every 40 seconds during the actual experiment.

Figure 16b illustrates the integral of the evolution curves to obtain cumulative evolved product amounts. Because the data are quantitative, the sum of these curves match the weight loss as determined by the TGA balance. Discrepancies occur because of components such as H₂ which cannot be seen by IR. When O₂ is introduced, the balance shows a net gain in weight due to O₂ chemisorption.

Determination of FG-DVC Model Parameters - The kinetic and composition parameters for the FG-DVC model are obtained from the TG/plus pyrolysis cycle. The pyrolysis cycle for Illinois No. 6 coal (Argonne premium sample) is presented in Fig. 17. Figure 17a presents the weight loss and temperature profile. Also presented (dashed line) is the sum of species (tar, CH₄, H₂O, CO₂, CO, SO₂, NH₃, C₂H₄, and COS). The sum of species is within a few percent of the weight loss.

The water evolution (Fig. 17b) consists of a low temperature moisture peak followed by a pyrolysis peak. To fit the wide pyrolysis peak by the FG submodel, three sources are used for H₂O. Each source evolves according to

$$dW_i/dt = k_i W_i(\text{char}) \quad (1)$$

where W_i is the gas species and W_i(char) is the amount of the functional group source remaining in the char. The rate constant, k_i is given by an Arrhenius expression of the form

$$k_i = A_i \exp\{-E_i \pm \sigma_i\}/RT \quad (2)$$

where A_i is the frequency factor, E_i the activation energy and σ_i the distribution in activation energies. Two sources are employed for CH₄, and three sources for CO and CO₂. Note the elimination of the calcite CO₂ evolution peak (Fig. 17d) and the increase in tar (Fig. 17c) for the demineralized coal.

To obtain the model parameters, the model is fit to the TG/plus data at three heating rates (3, 30, and 100°C/min). When there are multiple sources for a given species and the sources have overlapping peaks, the determination of parameters is not unique and some rules must be assumed. Based on chemical arguments, A is restricted between 10¹² and 10¹⁵ sec⁻¹. Also, the preexponential for a given species pool is assumed rank invariant based on the observed rank variation of the evolution curves. As the coal is increased in rank, the leading edges and the early peaks (Extra Loose or Loose pools) shift to higher temperatures while the trailing edge (Tight or Extra Tight pools) remain at the same temperature. An example of this is shown for water for five coals in Fig. 18a (16). From this figure it appears that the shift in the evolution curve with rank can be explained by the geological aging process. With increasing aging temperature and time, the maturation process gradually evolve the loosely bounded functional groups and leaves the tightly bounded groups intact.

The shift can be simulated by pyrolyzing a species described by a distribution of activation energies (Eq. 2) up to different bed temperatures. An example is shown in Fig. 18b. Starting with the evolution profile for Zap lignite, the coal is assumed to pyrolyze at 10°C/million years up to temperatures of (60, 120, 150, and 180°C). The resulting geologically aged samples is simulated using the TG/plus temperature profile and the predicted results are plotted. The curves for geological aging at 120, 150, and 180°C are similar to the actual TG/plus evolution curves shown in Fig. 18a for Illinois No. 6, Pittsburgh, No. 8, and Upper Freeport, respectively. Thus, the frequency factor is assumed to be constant as the rank increases, and the activation energy of the pool increased with increasing coal rank to fit the data. We find that the activation energy of tight pools generally change with rank much less than do the loose pools.

A typical comparison of theory and TG-FTIR experiments is shown in Fig. 19 for the Pittsburgh Seam coal for one heating rate. The amounts of the functional group pools are obtained from this procedure. The resolution of the hydrocarbon evolution into paraffins, olefins, ethane, ethylene, propane, and propylene is done in other experiments if required. Figure 20 compares the theory and experiment for three heating rates for weight loss, tar evolution, and methane evolution. The kinetic parameters are derived from these experiments. The agreement between the theory and experiment is quite good.

We have applied these curve fitting procedures for the eight Argonne coals according to the rules cited above (i.e., frequency factor between 10^{12} and 10^{15} /sec and constant for a given gas species pool independent of coal rank). Results for the rates for bond breaking, the evolution of methane (two pools), CO (three pools), CO₂ (three pools) and H₂O (three pools) are presented as a function of the coal's oxygen concentration in Fig. 21. As can be seen, there is a systematic increase in activation energy with increasing rank. The variation in activation energy is maximum for the loose pool and reduces as the activation energy increases. The amounts for these pools are presented in Fig. 22. There is a systematic variation in the amounts with rank.

Solvent Swelling, Extraction and NMR

Solvent swelling and extraction data for the Argonne coals are presented in Table 1. As discussed above, the extract yield is employed to determine the length of the chains (Monte Carlo) or the starting bond probabilities (percolation) used in the model. There appears to be some problem in employing this approach for the highest rank coals (Pocahontas and Upper Freeport). The swelling and extract yields for these coals in pyridine appears to be limited by weak crosslinking (other than hydrogen bonding) forces which are not eliminated by pyridine.

The solvent swelling ratio has been employed to determine the crosslink density (2,3,24-29). The various theories and values for the solvent interaction parameter (24-29) suggest that there are between 4 and 8 ring clusters between crosslinks, indicating a value of $\sigma + 1$ between 2.13 and 2.25 (32). NMR results of Solum et al. (5) for the number of bridges and loops suggest a value of $\sigma + 1$ of between 2 and 3, so a value in the neighborhood of 2.5 seems reasonable. However, the uncertainty of these determinations is too large to employ them in the model. The crosslink density is instead considered an adjustable parameter employed to fit the fluidity data.

Geissler Fluidity

As discussed above, the crosslink density controls the effective coordination number of the network, and hence the molecular weight distribution and amount of the fragments. For bituminous coals, it is the initial crosslink density which is important, since few new crosslinks are formed prior to pyrolysis. A recent theory for fluidity was developed based on the liquid fraction in the coal computed by the FG-DVC model (8,43). Measurements of the tar and the fluidity thus provide a constraint on the molecular distribution of the fragments and hence on the crosslink density.

Figure 23 presents a comparison of theory and experiment for four of the Argonne coals with the kinetic parameters fit from TG-FTIR data. The fitting procedure for fluidity and tar determines a unique combination of the crosslink density and donatable hydrogen.

Monomer Molecular Weight Distribution

The molecular weight distribution of the monomers is chosen based on the ring cluster size determined by NMR (5) and the results of the model checked with FIMS data (6).

RESULTS

Volatiles Evolution

A good test of the validity of using the TG-FTIR method over a range of low heating rates to obtain kinetic parameters is the ability to use the kinetic parameters to extrapolate to high heating rate conditions. Figure 24 presents results for Illinois No. 6 coal (obtained from Combustion Engineering) using the complete FG-DVC model and the most recent kinetic and composition parameters derived from the TG/plus (65). The predicted rates of evolution for each species are in good agreement with the observed rates except for water where moisture sometimes creates measurement errors. The data were obtained in the heated tube reactor where FT-IR emission and transmission measurements of coal particle temperatures determined the heating rate to be over 20,000 K/sec.

Char

A number of char characteristics can be measured and compared with the model. These include fluidity (already discussed in Section III), functional group composition, crosslink density, PMRTA, and extract yield. These are discussed below.

Functional Group Composition - The functional group composition can be determined by FT-IR (74-77) or NMR CP-MS with dipolar dephasing (5). A set of chars was prepared by heating Pittsburgh Seam coal up to temperatures of 200, 300, 400, 500, and 600°C at 30°C/sec and the chars were characterized (68). Figure 25 compares the theory with NMR and FT-IR measurements. The fractions of aliphatic and aromatic carbons are compared in Fig. 25a, and aliphatic, aromatic, methyl, and hydroxyl hydrogens in Fig. 25b. Figures 25c and 25d compare the theory and FT-IR measurements for the same quantities (except methyl and aliphatic hydrogen are lumped together). The tar yield (Fig. 26a), and methane yield (Fig. 26b) are presented for comparison. The model predictions are in excellent agreement with the data.

Crosslink Density - The application of the volumetric swelling ratio to obtain the changing crosslink density in the char was discussed in Section II. Comparison with theory was discussed in Ref. 7. Figure 26c compares the theory and experiment for the set of chars in Figs. 25 and 26. The agreement is good. Figure 27 compares the theory and experiment for two coals (Zap lignite and Pittsburgh Seam). The theory predicts the early crosslinking in Zap lignite (related to CO₂ evolution) not seen for the bituminous coal. The agreement between theory and experiment is good except that the increase in 1 - x for the Pittsburgh Seam coal in Fig. 27 is not predicted.

The NMR data also provide a direct measurement of the number of attachments per cluster (5). Figure 28 presents data (68) for total number of attachments (which includes peripheral groups, bridges, and loops), and just bridges and loops (B & L) as a function of final temperature for Pittsburgh Seam coal heated at 30°C/min to the indicated temperature. The FG-DVC model predicts the number of B & L. This quantity (near 2 for coal) is the coordination number, suggesting that coal is quite chain-like. There is little change in B & L up to 400°C. B&L increased at 500°C and above where crosslinking related to methane evolution is believed to occur.

Notice that the total number of attachments changes very little. This would be reasonable if the methane peripheral groups were replaced by bridges in substitution reactions. This is believed to be the reason for the correlation between methane evolution and crosslinking.

PMRTA - Proton magnetic resonance thermal analysis (PMRTA) is employed at CSIRO as an alternative to fluidity measurements. The measurement of proton mobility can distinguish protons on molecules free to rotate from protons on a rigid lattice. The molecules ability to rotate depends on its freedom from the network (i.e., it must be unattached or attached at only one place) and on the mobility of free molecules to rotate (which depends on the temperature). From the measured M_{2T} values, a "mobile" liquid fraction can be defined by the expression (72)

$$\text{Liquid Fraction} = \frac{M_{2T}(\text{room temperature}) - M_{2T}(T)}{M_{2T}(\text{room temperature})}$$

At sufficiently high temperature, when the free molecules have sufficient energy to rotate, this quantity should be equal to the FG-DVC liquid fraction. Figures 29a and 29d, compare the measured and predicted liquid fraction using both the Monte Carlo and percolation models. As expected, the theory and experiment do not agree at low temperature, but there is good agreement on the softening temperature, peak fluidity temperature, and solidification temperature. The liquid amounts in the two theories are defined differently and so the absolute amounts do not agree. Also shown for comparison are the fluidity and tar evolution curves for the same coal at a similar heating rate. The agreement between the data and both theories is good.

Extract Yields - Figure 30 compares the FG-DVC predictions to the data of Fong et al. (73) on total volatile yield and extract yield as a function of temperature in pyrolysis at 0.85 atm. The experiment was performed in a heated grid apparatus at heating rates of 640°C to 1018 K, with variable holding times and rapid cooldown. The predictions in Fig. 30 are in reasonable agreement with the data. The predicted extract yields are not as high as the measured yields. However, such high yields of extracts have not been duplicated by others, and there is some possibility that the extracted fraction also contains some colloidal material.

Weathering - Oxidation of a Pittsburgh Seam coal in our laboratory was performed at 80°C for 10, 20, and 62 days. In our model, the loss of fluidity with increasing oxygen concentration is related to the increase in CO₂ evolution and hence increases in low temperature crosslinking. To determine the CO₂ evolution, measurements were made in the TG-FTIR (78). The data in Fig. 31a shows that the low temperature CO₂ evolution was significantly increased after 10 days of oxidation, becoming comparable to that for Illinois No. 6. After 20 days, the early CO₂ evolution was larger than that for the Utah bituminous coal. After three months at 110°C the CO₂ evolution was comparable to that of a lignite. When these increased CO₂ yields were incorporated in the simulation for the oxidized Pittsburgh Seam coal's fluidity, the maximum fluidity was reduced. We compare our predicted maximum fluidity with the measurement of Wu et al. (79) for comparable coal and oxidation treatment in Fig. 31b. The agreement is quite reasonable.

Predicted Molecular Weight Distribution in Char - The dominant event in determining the char's properties is the starting and low temperature crosslinking behavior. Figures 32a and 32b compare the predicted molecular weight distributions in the char for Zap lignite and a Pittsburgh Seam bituminous coal. The bituminous coal (Fig. 32a) exhibits substantial fragmentation of tar precursors (n-mers 1-3), extracts (n-mers 4-10), and liquids (n-mers 11-100). On the other hand, the initial crosslink density in the lignite, and the subsequent increase due to CO₂ related crosslinking, allows almost no n-mers except monomers, dimers, and trimers to be formed (Fig. 32b). These predictions of the model are related to the extract yields, PMRTA analysis fluidity, and tar yields.

Tar

Molecular Weight Distribution - The tar is evolved from the lightest fractions of the metaplast and depends on the metaplast distribution and the transport. This is illustrated in Fig. 32c and 32d, which are the predicted tar distribution for a bituminous coal and a lignite (two cases discussed above). For the bituminous coal, the upper molecular weight is limited only by the vapor pressure for the large molecules. For the lignite, the metaplast distribution limits the amount and molecular weight distribution.

Figures 33c, and 33d show measurements for the Pittsburgh Seam bituminous coal and the Beulah, Zap lignite pyrolyzed in the FIMS apparatus. The data have been summed over 50 amu intervals. While the Pittsburgh bituminous coal shows a peak intensity at about 400 Daltons, the lignite peak is at 100 Daltons. The predicted average tar molecular weight distributions are in good agreement with FIMS data as shown in Figs. 33a and 33b. Since both tar distributions are from the same monomer distribution, the enhanced drop off in amplitude with increased molecular weight for the lignite compared to the bituminous coal must be due to early crosslinking and transport effects in the lignite.

Pressure Effects - The prediction effect of pressure on the tar molecular weight distribution is illustrated in Figs. 34a and 34b. Pressure enters the model through the transport assumption. The internal transport rate is inversely proportional to the ambient pressure. The reduced transport rate reduces the evolution rate of the heavier molecules. Therefore, the average molecular weight and vaporization "cutoff" decrease with increasing pressure. The trends are in agreement with observed tar molecular weight distributions shown in Figs. 34c and 34d. The spectra are for previously formed tars that have been collected and analyzed in a FIMS apparatus (6). The low values of intensity between 100 and 200 Daltons are believed to be due to loss of these components due to their higher volatility.

Yield - The tar yields are measured in the TG-FTIR. Figure 35 compares the measured and predicted yield as a function of temperature. The agreement is good except for the low temperature evolution

of guest molecules, which is not well predicted in the standard model. Improvements to predict this early peak have been made (8).

Network Parameters

Figure 36 presents the adjustable network parameters which have been chosen to fit the tar evolution and fluidity data as functions of the oxygen concentration. The oligomer length and the molecular weight between crosslinks increase smoothly with rank. The concentration of available hydrogen for ring stabilization has a maximum for the high volatile bituminous coals.

In Fig. 37, we compare the predicted and measured extract yield and the predicted and estimated molecular weight between crosslinks. The crosslink density for the bituminous coals is within the range of measured values. The model, however, requires a high molecular weight between crosslinks, M_c , for Pocahontas and Upper Freeport, while the solvent swelling ratios would indicate a low M_c value. The model also requires a high extract yield for Upper Freeport while the measured yields are low. There may be an additional kind of weak crosslink for high rank coals, possibly associated with the aromatic-aromatic interactions suggested by Larsen (80). When the Upper Freeport coal is heated to 300°C and then cooled the solvent swelling ratio increases from 1.32 to 2.13 and the extract yield from 10.4 to 21%, suggesting that this treatment may loosen some of these weak bonds non-reversibly.

SUMMARY AND CONCLUSIONS

The paper poses the question, can coal science be predictive? The answer is yes for coal thermal decomposition in particles small enough to be isothermal. It is possible to construct a model based on reasonable assumptions to predict almost all of the observed behavior. The model has only one parameter which is adjusted for the process conditions. This is the internal pressure in the transport submodel. All other model parameters of the coal are fixed for each coal. The model has composition and kinetic parameters to describe the evolution of each individual gas species. These can be determined in TG-FTIR experiments and exhibit a systematic variation with rank. There are three network parameters in the Monte Carlo version of the model, the chain length, the crosslink density, and the available donatable hydrogen. A similar set of network parameters is used in the percolation theory. These are adjusted to fit the TG-FTIR, tar yields, extract yields, and fluidity. These also exhibit a systematic variation with rank.

The paper explores the six concepts which are the foundation of the FG-DVC model:

- 1) **The decomposition of functional group sources in the coal yield the light gas species in thermal decomposition.** The amount and evolution kinetics can be measured by TG-FTIR, the functional group changes by FT-IR and NMR. There is good agreement between the model and NMR, FT-IR, and TG-FTIR measurements on a Pittsburgh Seam coal heated at 30°C/min and for gas evolution for a lignite and an Illinois No. 6 bituminous coal at 30°C/min and 20,000°C/sec.
- 2) **The decomposition of a macromolecular network yields tar and metaplast.** The amount and kinetics of the tar evolution can be measured by TG-FTIR and the molecular weight by FIMS. The kinetics of metaplast formation and destruction can be measured by solvent extraction, by Geissler plastometer and proton magnetic resonance thermal analysis (PMRTA). Reasonable agreement has been demonstrated for solvent extract of a Pittsburgh Seam coal pyrolyzed at 30°C/min and 640°C/sec. Good agreement was shown for four of the Argonne coal samples for fluidity by Geissler plastometer, and for one coal by PMTRA.
- 3) **The molecular weight distribution of the metaplast depend on the network coordination number.** The coordination number can be determined by solvent swelling and NMR.
- 4) **The network decomposition is controlled by bridge breaking and the amount of bridge breaking is limited by the available donatable hydrogen.**

5) **The network solidification is controlled by crosslinking.** The changing crosslink density can be measured by solvent swelling and NMR. Crosslinking appears to occur with evolution of both CO₂ (prior to bridge breaking) and CH₄ after bridge breaking. Thus, low rank coals (which form a lot of CO₂) crosslink prior to bridge breaking and are thus thermosetting. High volatile bituminous coals (which form little CO₂) undergo significant bridge breaking prior to crosslinking and become highly fluid. Weathering, which increases the CO₂ yield, causes increased crosslinking and lowers fluidity. There is good agreement between the predicted and measured crosslink densities and fluidities in the FG-DVC model in which crosslinks are correlated with CO₂ and CH₄ gas evolution.

6) **The evolution of tar is controlled by mass transport in which the tar molecules evaporate into the light gas species and are carried out of the coal at rates proportion to their vapor pressure and the volume of light gases.** High pressures reduces the volume of light gases and hence reduces the yield of heavy molecules with low vapor pressure. These changes can be studied with FIMS. The changes in tar yield and molecular weight distribution with pressure have been accurately predicted using the vapor pressure law, of Suuberg and coworkers.

The paper describes how the coal kinetics and composition parameters are obtained by TG-FTIR, solvent swelling, solvent extraction, Geissler plastometer data, NMR data and FIMS data. The model is compared to a variety of experimental data in which heating rate (0.05 to 20,000 °C/sec), temperature (100 to 1600 °C), and pressure (vacuum to 100 atm) are all varied. There is good agreement with theory (both Monte Carlo and percolation) and most of the data available from our laboratory and in the literature.

The network parameters employed in the model have been presented. The results suggest that there is some form of weak crosslinks for Pocahontas and Upper Freeport coal.

While the experimental results and the model are consistent with the suggested processes, the chemical reactions for bridge breaking, crosslinking, and functional group decomposition are not defined in detail. Also, there is only sparse data to validate the transport assumption and the internal pressure in the particle is an adjustable parameter of the model.

ACKNOWLEDGEMENTS

The authors wish to acknowledge the following organizations for their support over the last ten years: U.S. Department of Energy, Morgantown Energy Technology Center, U.S. Department of Energy, Pittsburgh Energy Technology Center, National Science Foundation, and Gas Research Institute. The authors also wish to acknowledge the extensive contribution from many coauthors who have collaborated on the various aspects of this work: Robert Carangelo, James Markham, Philip Best, Erik Kroo, Yan Ping Zhang, Rosemary Bassilakis, Marie DiTaranto, Girish Deshpande, Po-Liang Chien, H.H. King, Tom Squires, and Kevin Squire who worked at Advanced Fuel Research, Inc., Meredith Colket from United Technologies Research Center, Douglas Smoot and Scott Brewster from Brigham Young University, Eric Suuberg from Brown University, Ronald Pugmire, David Grant, and Mark Solum from the University of Utah, Donald McMillen and Ripudaman Malhotra from SRI International, Rashid Khan from Texaco, Tom Fletcher from Sandia National Laboratory, Leo Lynch and Richard Sakurovs from CSIRO, Bernie Gerstein from Iowa State University, Jean Whelan from Woods Hole Oceanographic Institute, Harold Schobert and Caroline Burgess at Penn State University, Garry Vail, Fred Baudais, Michel Baillargeon, Daniel Gravel from Bormer, Inc. and Dennis Gerson from IBM Instruments.

REFERENCES

1. Solomon, P.R., Serio, M.A., Carangelo, R.M., Bassilakis, R., Gravel, D., Baillargeon, M., Baudais, F., and Vail, G., *Energy and Fuels*, 1990, 4(3), 319.
2. Green, T.K., Kovac, J., and Larsen, J.W., *Fuel*, 1984, 63, 935.
3. Green, T.K., Kovac, J., and Larsen, J.W., *Coal Structure*, R.A. Meyers, Ed., Academic, NY, 1982, p. 199.
4. The Geissler Plastometer data was supplied by Mr. George Engelke from Commercial Testing

- and Engineering Company.
5. Solum, M.A., Pugmire, R.J., and Grant, D.M., *Energy & Fuels*, 1989, 3, 187.
 6. St. John, G.A., Buttrill, S.E., Jr., and Anbar, M., ACS Symposium Series 71, American Chemical Society, Washington, DC, 1978, p. 223.
 7. Solomon, P.R., Hamblen, D.G., Carangelo, R.M., Serio, M.A., and Deshpande, G.V., *Energy and Fuel*, 1988, 2, 405.
 8. Solomon, P.R., Serio, M.A., Hamblen, D.G., Yu, Z.Z., and Charpenay, S., *ACS Div. of Fuel Chem. Preprints*, 1990, 35(2), 479.
 9. Solomon, P.R., in *Coal Structure*, Advances in Chemistry Series, 1981, 192, 95.
 10. Solomon, P.R. and Hamblen, D.G., "Pyrolysis", in *Chemistry of Coal Conversion*, (R.H. Schlosberg, Editor), Plenum, New York, NY, 1985, pp. 121-251.
 11. Solomon, P.R., Hamblen, D.G., Carangelo, R.M., and Krause, J.L., *Nineteenth Symposium (Int) on Combustion*, 1139, The Combustion Institute, Pittsburgh, PA, 1982, 1139.
 12. Serio, M.A., Hamblen, D.G., Markham, J.R., Solomon, P.R., *Energy and Fuel*, 1987, 1, 138.
 13. Solomon, P.R. and King, H.H., *Fuel*, 1984, 63, 1302.
 14. Squire, K.R., Carangelo, R.M., DiTaranto, M.B., and Solomon, P.R., *Fuel*, 1986, 65, 833.
 15. Solomon, P.R., Hamblen, D.G., Carangelo, R.M., Serio, M.A. and Deshpande, G.V., *Combustion and Flame*, 1988, 71, 137.
 16. Solomon, P.R., Serio, M.A., Carangelo, R.M., Bassilakis, R., Yu, Z.Z., Charpenay, S., and Whelan, J., "Analysis of Coal by TG-FTIR and Pyrolysis Modeling", presented at the Pyrolysis '90 Meeting in Holland, June 1990, to be published in *Journal of Analytical and Applied Pyrolysis*.
 17. Suuberg, E.M., Peters, W.A., and Howard, J.B., *Seventeenth Symposium (Int) on Combustion*, The Combustion Institute, Pittsburgh, PA 1979, 117.
 18. Gavalas, G.R., Cheong, P.H., and Jain, R., *Ind. Eng. Chem. Fundam.*, 1981, 20, 113.
 19. Gavalas, G.R., Cheong, P.H., and Jain, R., *Ind. Eng. Chem. Fundam.*, 1981, 20, 122.
 20. Xu, W.C. and Tomita, A., *Fuel*, 1987, 66, 627.
 21. van Krevelen, D.W., *Coal*, Elsevier, Amsterdam, 1961.
 22. Solomon, P.R., Squire, K.R., and Carangelo, R.M., *Int. Conf. on Coal Science*, Pergamon, Sydney, Australia, 1985, p. 945.
 23. Brenner, D., *Fuel*, 1985, 64, 167.
 24. Lucht, L.M. and Peppas, N.A., *Fuel*, 1987, 66, 803.
 25. Lucht, L.M., Larsen, J.M., and Peppas, N.A., *Energy & Fuels*, 1987, 1, 56.
 26. Larsen, J.W., *ACS Fuel Chem. Div. Preprints*, 1985, 30(4), 444.
 27. Green, T., Kovac, J., Brenner, D., and Larsen, J., *Coal Structure*, (R.A. Meyers, Ed.), Academic, NY, 1982, p. 199.
 28. Hall, P.J., Marsh, H., and Thomas, K.M., *Fuel*, 1988, 67, 863.
 29. Sanada, Y. and Honda, H., *Fuel*, 1966, 45, 295.
 30. Suuberg, E.M., Yoshi, O., and Deevo, S., *ACS Div. Fuel Chem. Prepr.*, 1988, 33(1), 387.
 31. Gavalas, G.R., *Coal Pyrolysis*, Elsevier, NY, 1982 p. 51
 32. Solomon, P.R., Hamblen, D.G., Yu, Z.Z., and Serio, M.A., *Fuel*, 1990, 69, 754.
 33. Niksa, S., and Kerstein, A.R., *Combustion and Flame*, 1986, 66, 95.
 34. Niksa, S., *Combustion and Flame*, 1986, 66 111.
 35. Niksa, S. and Kerstein, A.R., *Fuel*, 1987, 66, 1389.
 36. Grant, D.M., Pugmire, R.J., Fletcher, T.H., and Kerstein, A.R., *Energy & Fuels*, 1989, 3, 175.
 37. Nelson, P.F., *Fuel*, 1987, 66, 1264.
 38. Calkins, W.H., Hagaman, E., and Zeldes, H., *Fuel*, 1984, 63, 1113.
 39. Calkins, W.H., and Tyler, R.J., *Fuel*, 1984, 63, 1119.
 40. Calkins, W.H., *Fuel*, 1985, 64, 1125.
 41. Calkins, W.H., Hovsepian, B.K., Drykacz, G.R., Bloomquist, C.A.A., and Ruscic, L., *Fuel*, 1984, 63, 1226.
 42. Niksa, S., *AIChE J.*, 1988, 34, 790.
 43. Solomon, P.R., Best, P.E., Yu, Z.Z., and Deshpande, G.V., *ACS Div. of Fuel Chem. Preprints*, 1989, 34(3), 895.
 44. Suuberg, E.M., Lee, D., and Larsen, J.W., *Fuel*, 1985, 64, 1668.
 45. Suuberg, E.M., Unger, P.E., and Larsen, J.W., *Energy and Fuels*, 1987, 1, 305.
 46. Bockrath, B.C., Illig, E.G., and Eassell-Bridger, W.D., *Energy & Fuels*, 1987, 1, 227.
 47. Solomon, P.R., Serio, M.A., Deshpande, G.V., and Kroo, E., *Energy & Fuels*, 1990, 4(1), 42.

48. Solomon, P.R., "Coal Structure and Thermal Decomposition", in New Approaches in Coal Chemistry, ACS Symposium Series 169, 1981, 61.
49. Brown, J.K., Dryden, I.G.C., Dunevein, D.H., Joy, W.K., and Pankhurst, K.S., *Inst. Fuel*, 1958, 31, 259.
50. Orning, A.A. and Greifer, B., *Fuel*, 1956, 35, 318.
51. Freihaut, J.D., Proscia, W.M., and Seery, D.J., *Energy & Fuels*, 1989, 3, 692.
52. Anthony, D.B. and Howard, J.B., *AIChE J.*, 1976, 22, 625.
53. Solomon, P.R., Serio, M.A., Carangelo, R.M., and Markham, J.R., *Fuel*, 1986, 65, 182.
54. Solomon, P.R. and Serio, M.A., "Evaluation of Coal Pyrolysis Kinetics", in Fundamentals of the Physical-Chemistry of Pulverized Coal Combustion, J. Lahaye and G. Prado, Eds.), Martinus Nijhoff, 1987, 126.
55. Kobayashi, H., Howard, J.B., and Sarofim, A.F., *Sixteenth Symposium (Int) on Combustion*, The Combustion Institute, Pittsburgh, PA, 1977, 411.
56. Solomon, P.R., and Colket, M.B., *Seventeenth Symposium (Int) on Combustion*, The Combustion Institute, Pittsburgh, PA, 1979, 131.
57. Anthony, D.B., Howard, J.B., Hottel, H.C., and Meissner, H.P., *Fifteenth Symposium (Int) on Combustion*, The Combustion Institute, Pittsburgh, PA, 1974, 1303.
58. Badzioch, S., and Hawksley, P.G., *Ind. Eng. Chem. Proc. Des., Dev.*, 1970, 9, 521.
59. Solomon, P.R., Fletcher, T.H., and Pugmire, R.J., Progress in Coal Pyrolysis, Pittsburgh Coal Conference, (Sept. 10-14, 1990).
60. Solomon, P.R., Serio, M.A., and Suuberg, E.M., Review of Coal Pyrolysis: Experiments, Kinetic Rates, and Mechanisms, Progress in Energy and Combustion Science, submitted (1990).
61. Fletcher, T.H., *Combustion and Flame*, 1989, 78, 223.
62. Fletcher, T.H., *Combust. Sci. and Tech.*, 1989, 63, 89.
63. Freihaut, J.D. and Proscia, W.M., *Energy & Fuels*, 1989, 3(5), 625.
64. Solomon, P.R., Serio, M.A., and Markham, J.R., Kinetics of Coal Pyrolysis, Int. Conference on Coal Science Proceedings, IEA, Tokyo, Japan, p. 575, (October 23-27, 1989).
65. Serio, M.A., Solomon, P.R., Charpenay, S., Yu, Z.Z., and Bassilakis, R., *ACS Div of Fuel Chem. Preprints*, 1990, 35(3), 808.
66. Burnham, A.K., Oh, M.S., Crawford, R.W., and Samoun, A.M., *Energy & Fuel*, 1989, 3, 42.
67. Stein, S.E., Robauch, D.A., Alfieri, A.D., and Miller, R.E., *J. Am. Chem. Soc.*, 1982, 104, 6567.
68. Solum, M.S., Pugmire, R.J., Grant, D.M., Fletcher, T.H. and Solomon, P.R., Studies of Coal Char Structure Evolution: 1. Solid State ¹³C NMR, to be submitted, (1989).
69. Lynch, L.J., Sakurovs, R., Webster, D.S., and Redlich, P.J., *Fuel*, 1988, 67, 1036.
70. Lynch, L.J., Webster, D.S., Sakurovs, R., Barton, W.A., and Maher, T.P., *Fuel*, 1988, 67, 579.
71. Barton, W.A. and Lynch, L.J., *Energy & Fuels*, 1989, 3, 402.
72. Dr. Richard Sakurovs, personal communications.
73. Fong, W.S., Peters, W.A., and Howard, J.B., *Fuel*, 1986, 65, 251.
74. Sobkowwiak, M., Riesser, B., Given, R., and Painter, P., *Fuel*, 1984, 63, 1245.
75. Riesser, B., Starsinic, M., Squires, E., Davis, A., and Painter, P., *Fuel*, 1984, 63, 1253.
76. Solomon, P.R. and Carangelo, R.M., *Fuel*, 1988, 67, 949.
77. Solomon, P.R., and Carangelo, R.M., *Fuel*, 1982, 61, 663.
78. Solomon, P.R., Best, P.E., Yu, Z.Z., and Charpenay, S., "A Macromolecular Network Model for Coal Fluidity", to be submitted to *Fuel*, (1990).
79. Wu, M.M., Robbins, G.A., Winschel, R.A., and Burke, F.P., *Energy & Fuels*, 1988, 2, 150.
80. Larsen, J.W., *ACS Div. of Fuel Chem. Preprints*, 1988, 33(1), 400.

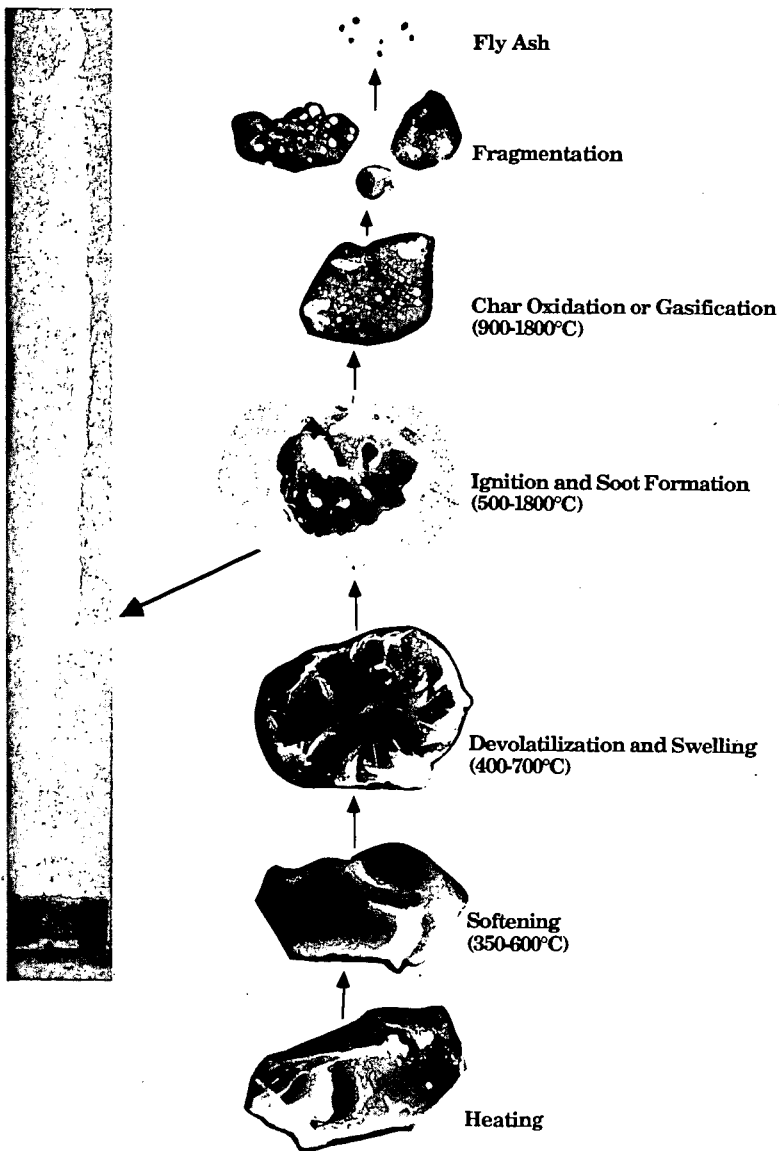


Figure 1. Processes in Coal Conversion.

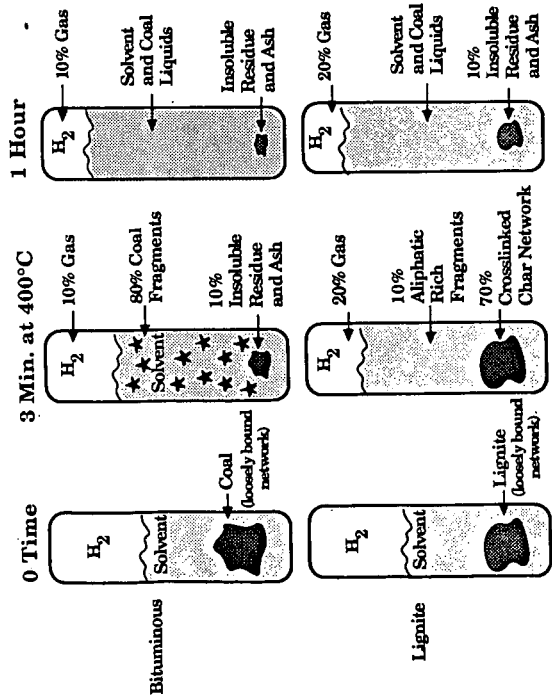


Figure 2. Process in Liquefaction.

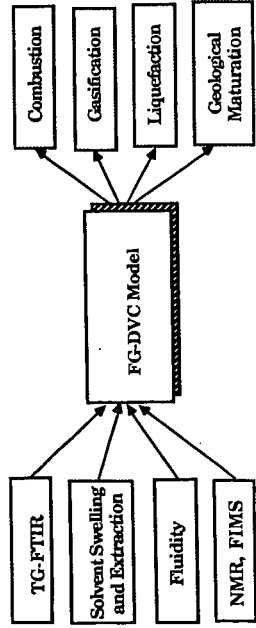


Figure 3. Coal Thermal Decomposition Model.

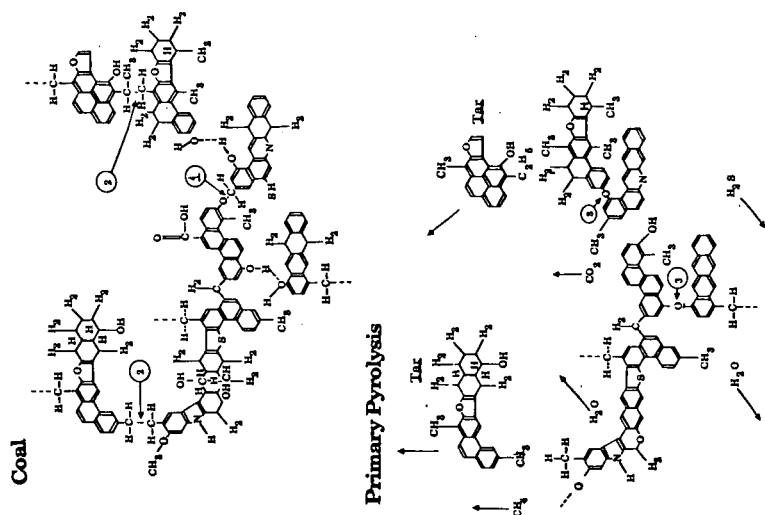


Figure 4. Hypothetical Model for Pittsburgh Seam Coal. a) Starting Coal, and b) During Pyrolysis.

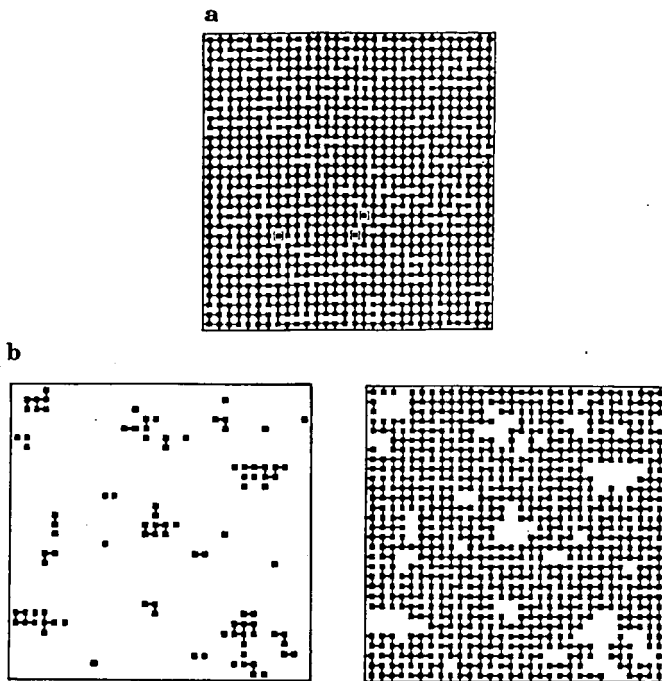


Figure 5. Monte Carlo Calculations for Coordination Number 4. a) 20% Broken Bridges, and b) 45% Broken Bridges (From Ref. 36).

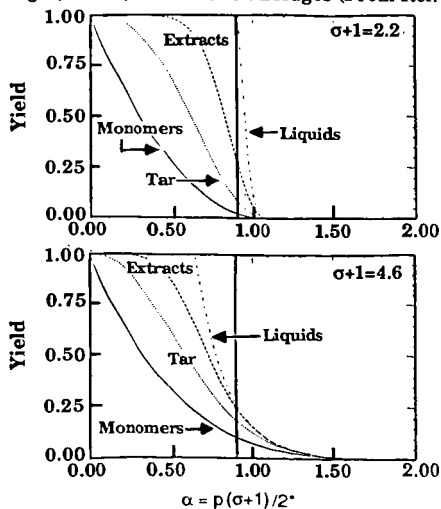


Figure 6. Percolation Theory Predictions for Pyrolysis Products for Two Coordination Numbers.

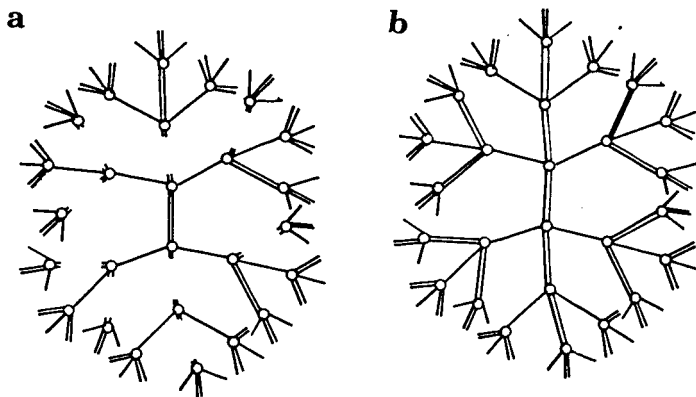


Figure 7. Bethe Lattice for Two- σ Model with $\sigma_1=1$ (shown as single bonds). a) Fully Linked Case ($p=q=1$) is like One- σ Model with $\sigma=3$. With Most Double Bands Representing the Crosslinks not yet Formed to Represent the Starting Coal. The Lattice is Like One- σ Model with $\sigma=1$, Linear Chains.

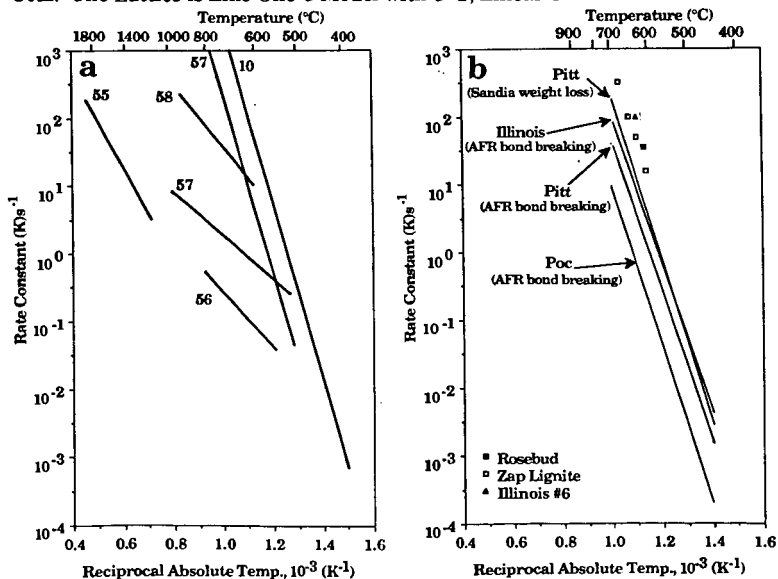


Figure 8. Kinetic Rate Constants for Weight Loss or Bridge Breaking. a) Extremes of Literature Rates from Experiments in which Particle Temperatures were not Directly Measured. b) More Recent Rates from Experiments in which Particle Temperatures were Measured.

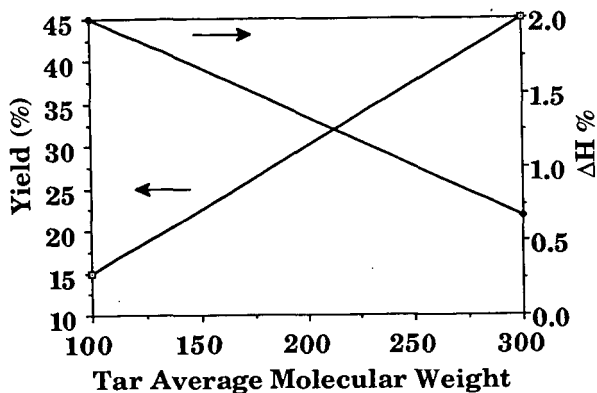


Figure 9. Yield and Hydrogen Concentration of Tar (.3% H available).

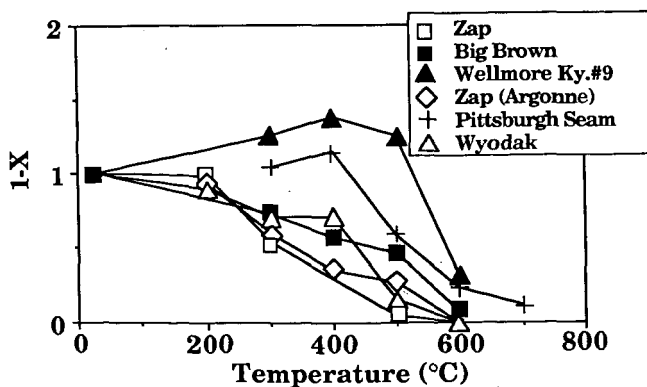


Figure 10. Comparison of Solvent Swelling Ratios for Coals of Various Ranks at a Series of Final Pyrolysis Temperatures at a Heating Rate of 30°C/min to Final Temperature.

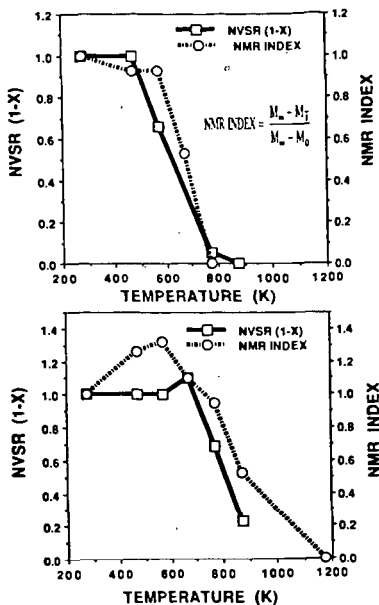


Figure 11. Comparison of NMR and Swelling Data for: a) Zap Lignite and b) Pittsburgh No. 8.

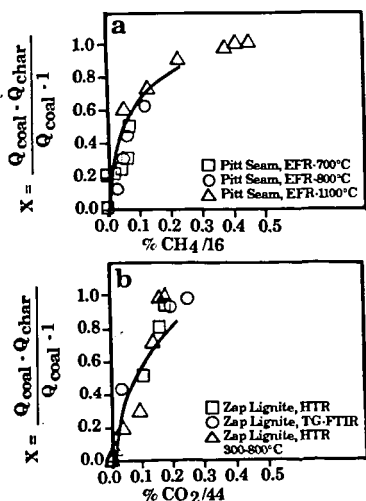


Figure 12. Measured and Calculated Normalized Volumetric Swelling Ratio (VSR) for Coal and Chars: a) Pittsburgh Seam Bituminous Coal Plotted Against the Methane Yield; b) Zap North Dakota Lignite Plotted Against the CO_2 Yield. VSR_{min} is the Value Achieved when Crosslinking is Complete. The Chars were Prepared in an Entrained Flow Reactor (EFR), a Heated Tube Reactor (HTR), and a Thermogravimetric Analyzer with Evolved Product Analysis by FT-IR (TG-FTIR) as Described in Ref.58.

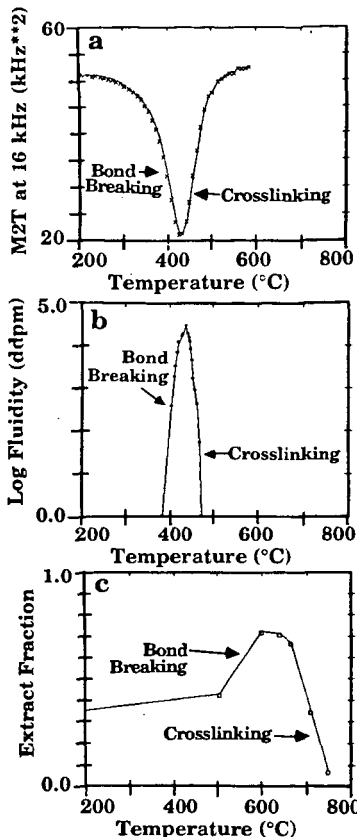
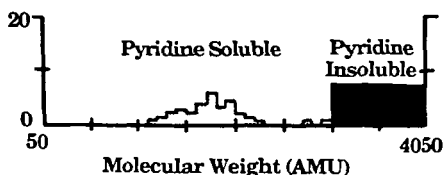
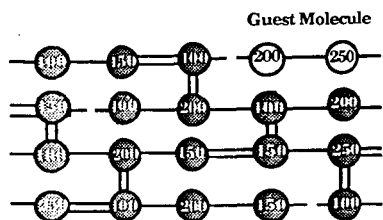
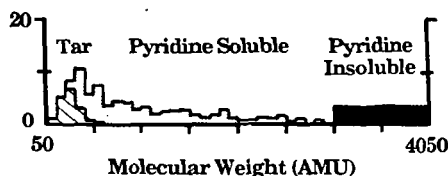
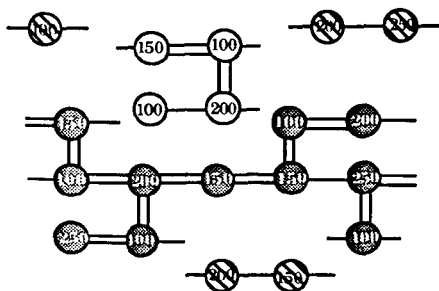


Figure 13. Experiments that Exhibit Bond Breaking and Crosslinking for Pittsburgh Seam Coal. a) PMRTA at $4^\circ\text{C}/\text{sec}$ (data of Sakurov) and LYNCH (72), b) Fluidity by Geissler at $3^\circ\text{C}/\text{sec}$ (data of Commercial Testing and Engineering (4) and c) Extract Yield at $640^\circ\text{C}/\text{sec}$ (data of Fong et al. (73).

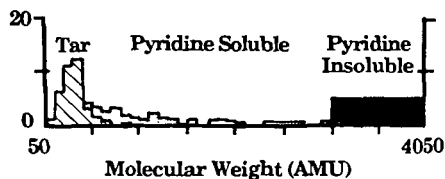
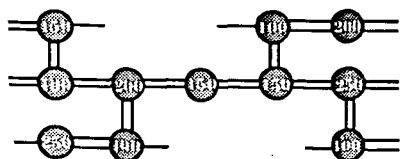
a. Starting Molecule



b. During Tar Formation



c. Char Formed



Tar  Char  P.S. Char  P.I.

Figure 14. Representation of Coal Molecule in the DVC Simulation and Corresponding Molecular Weight Distribution. In the Molecule, the Circles Represent Monomers (ring clusters and peripheral groups). The Molecular Weight Shown by the Numbers is the Molecular Weight of the Monomer Including the Attached Bridges. The Single-Line Bridges are Breakable and can Donate Hydrogen. The Double-line Bridges are Unbreakable and do not Donate Hydrogen. The Molecular Weight Distribution of the Coal, Tar, and Chars are Shown as a Histogram at the Right. The Histogram is Divided into Tar and Char with Pyridine-soluble and Pyridine-insoluble Fractions. The Area Under the Histogram Corresponds to the Weight Percent of the Oligomers. (From Ref. 58).

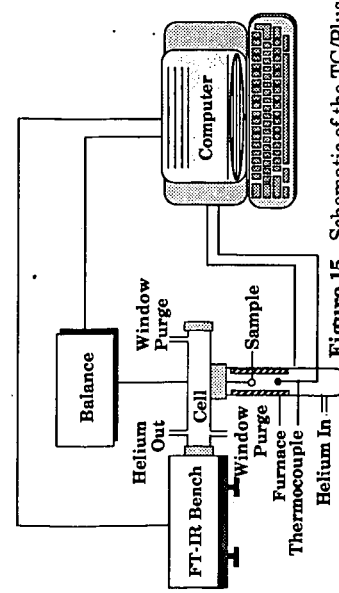


Figure 15. Schematic of the TG/Plus.

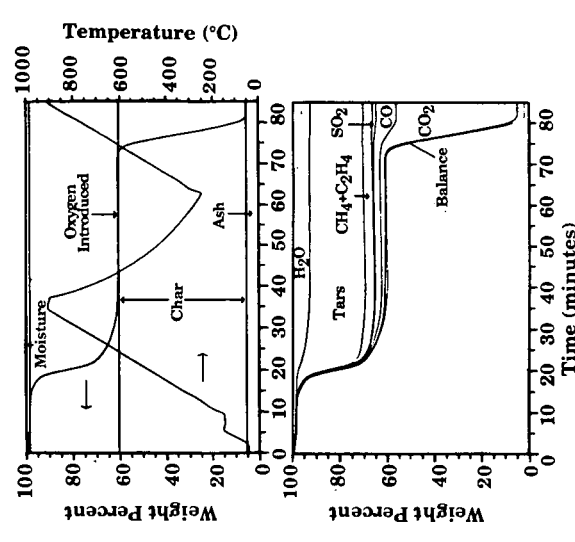


Figure 16. Thermogram and Quantitative Breakdown of Evolved Gases for Pittsburgh Seam Coal.

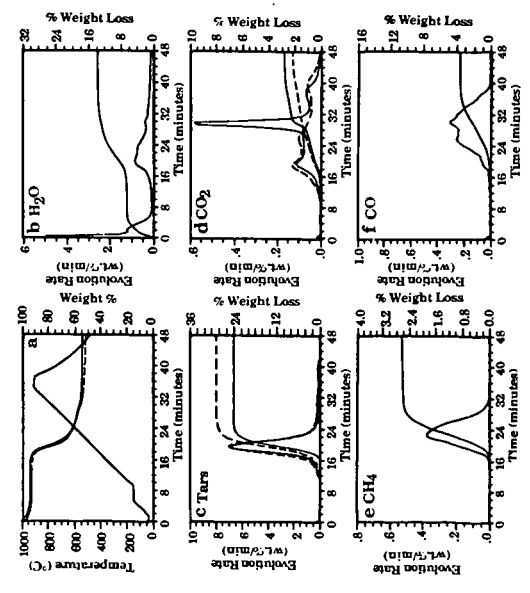


Figure 17. TG-FTIR Analysis of Raw and Demineralized Illinois No. 6 Coal During the Pyrolysis Cycle. a) Weight Loss (solid), Sum of Evolved Products (dashed), and Temperature Profile; b) H₂O Evolution Rate and Integrated Amount Evolved; c) Tar Evolution Rate and Integrated Amount Evolved (raw coal (solid line); demineralized coal (dashed line)); d) CO₂ Evolution Rate and Integrated Amount Evolved (raw coal (solid line); demineralized coal (dashed line)); e) CH₄ Evolution Rate and Integrated Amount Evolved; f) CO Evolution Rate and Integrated Amount Evolved. All Weight Losses are on an as Received Basis.

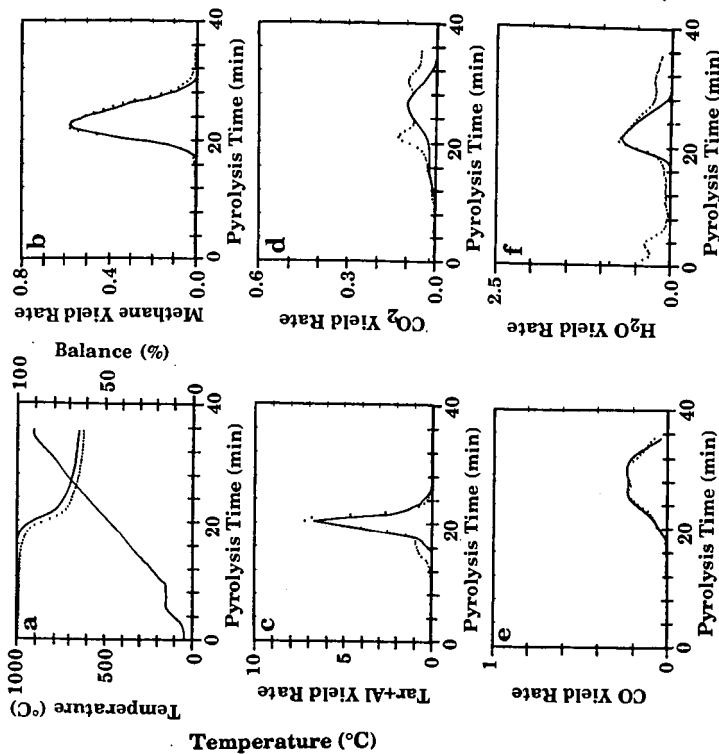


Figure 19. Data from TG-FTIR Heating Rates (---) and Predictions of FG-DVC Model for Pittsburgh No. 8 Bituminous Coal at 30°C/min. a) Weight Loss and Temperature; b) Methane; c) Tar + Aliphatic Gases; d) CO₂; e) CO; f) H₂O.

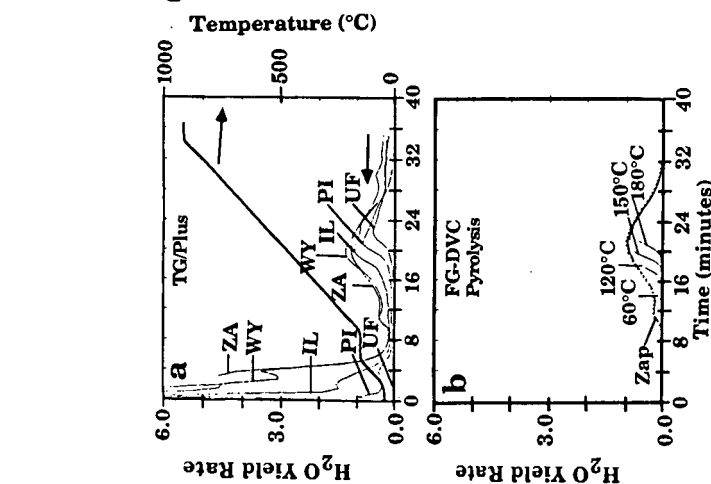


Figure 18. Evolution Curves for H₂O Measured in a) TG/Plus and b) FG-DVC Predictions for Five Coals from the Argonne Premium Sample Collected at 30°C/min. (UF-Upper Freeport, PI-Pittsburgh, IL-Illinois, WY-Wyodak, ZA-Zap Lignite).

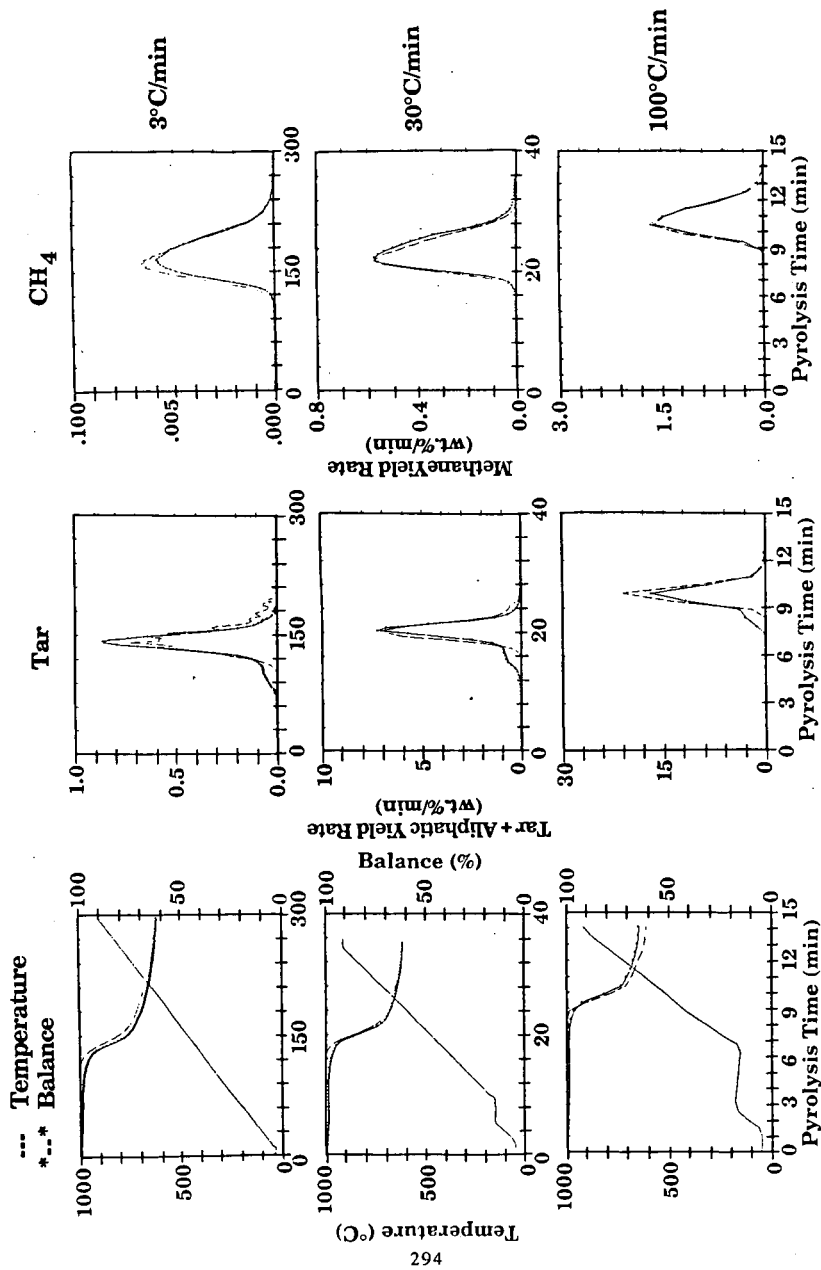


Figure 20. Kinetic Analysis at Three Heating Rates for Pittsburgh Seam Coal. Comparison of Theory (---) and Data (***)

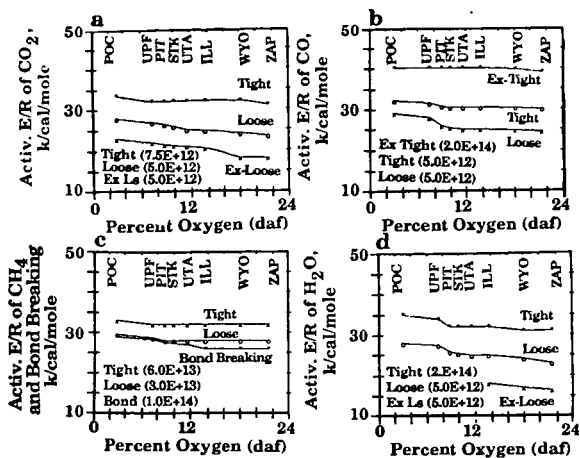


Figure 21. Activation Energies for Functional Group Pools as a Function of the Coal's Oxygen Concentration. The Frequency Factors are Shown in Parenthesis. a) CO₂ Tight, CO₂ Loose and CO₂ Ex-Loose, b) CO Ex-Tight, CO Tight and CO Loose, c) CH₄ Loose, CH₄ Tight and Bond Breaking, and d) H₂O Tight, H₂O Loose and H₂O Ex-Loose.

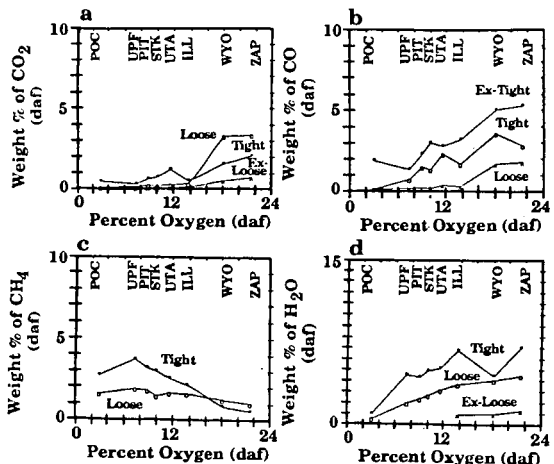


Figure 22. Amounts for Functional Group Pools as a Function of the Coal's Oxygen Concentration. a) CO₂ Tight, CO₂ Loose and CO₂ Ex-Loose, b) CO Ex-Tight, CO Tight and CO Loose, c) CH₄ Loose, CH₄ Tight and CH₄ Ex-Loose, and d) H₂O Tight, H₂O Loose and H₂O Ex-Loose.

Table 1 - Extract Yields and Volumetric Swelling Ratio (VSR) for Argonne Coals

Coal	Pyridine Extract DAF %	VSR Vacuum Dried
North Dakota	5.4	2.7
WY	10.7	2.7
WV	18.3	2.3
UT	22.5	2.7
Pitt	27.7	2.3
Ill No. 6	35.7	2.5
Poc	1.0	1.1
UF	10.4	1.3

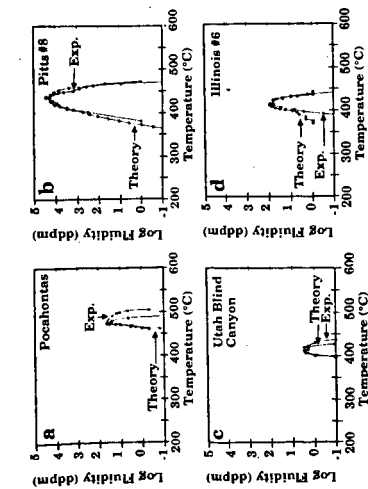


Figure 23. Measured and Predicted Fluidity for Four Argonne Coals.

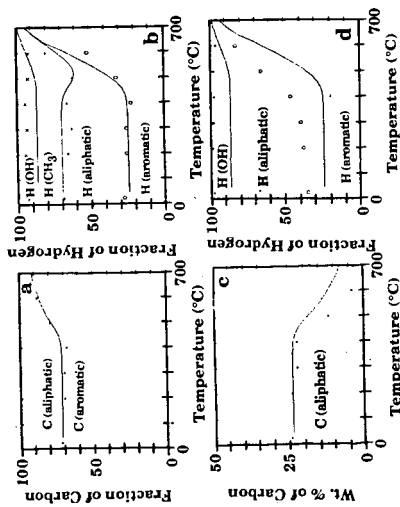


Figure 25. Comparison of Measured and Predicted Functional Group Composition of Pittsburgh Seam Char Heated at 30°C/min to the Indicated Temperature. a) Carbon Distribution by NMR, b) Hydrogen Distribution by NMR, c) Weight Percent Aliphatic Carbon by FT-IR, and d) Hydrogen Distribution by FT-IR. Data from Solum et al. (68).

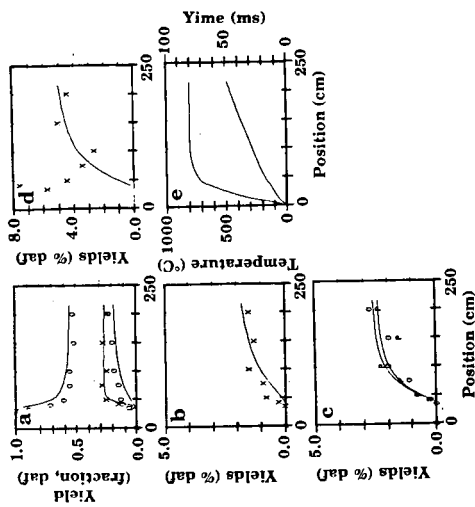


Figure 24. Predictions of FG-DVC Model for Illinois No. 6 Coal Pyrolyzed in the Heated Tube Reactor. a) Char, Tar and Gas, b) Methane, c) Olefins and Paraffins, d) Water and e) Time and Temperature. Data of Solomon et al. (53).

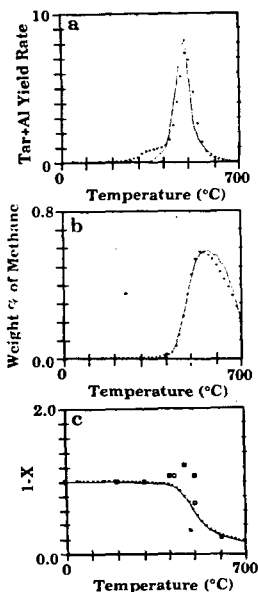


Figure 26. Comparison of Measured and Predicted Pyrolysis Behavior of Pittsburgh Seam Char Heated at 30°C/min to the Indicated Temperature. a) Tar Yield, b) Methane Yield, and c) Solvent Swelling Ratio.

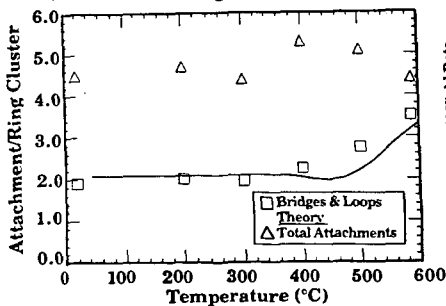


Figure 28. Comparison of Theory with NMR Data for Attachments to Ring Clusters (data from University of Utah).

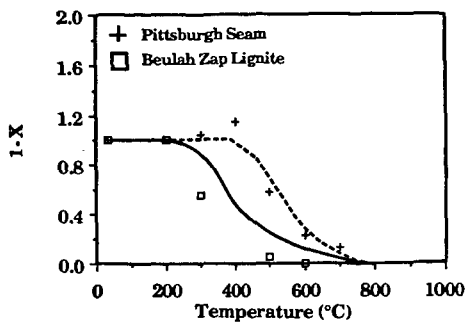


Figure 27. Comparison of Measured and Predicted Normalized Volumetric Swelling Ratio as a Function of Temperature for a Lignite and a Bituminous Coal.

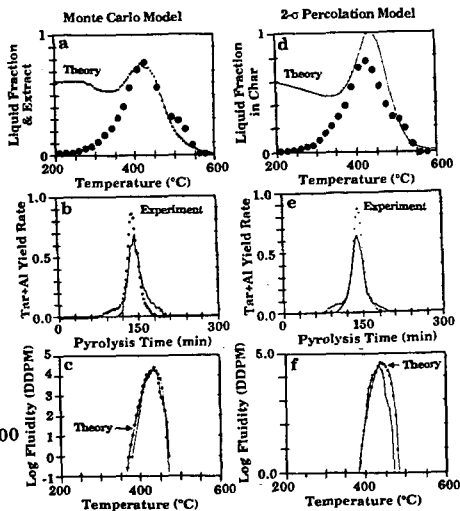


Figure 29. Comparison of Monte Carlo and 2- σ Percolation Theory for Liquid Fraction, Tar Yield and Fluidity for Pittsburgh No. 8 Bituminous Coal at 3°C/min.

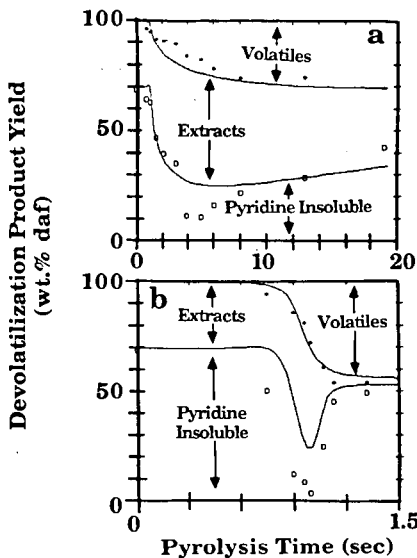


Figure 30. Comparison of FG-DVC Model Predictions with the Data of Fong et al. (73) (symbols) for Pittsburgh Seam Coal. a) 813K @ 470K/s and b) 1018K @ 640K/s. P=0.85 atm. The Solid Lines Assumes Transport by Eq. 4 ($\Delta P=0$ atm) and No External Transport.

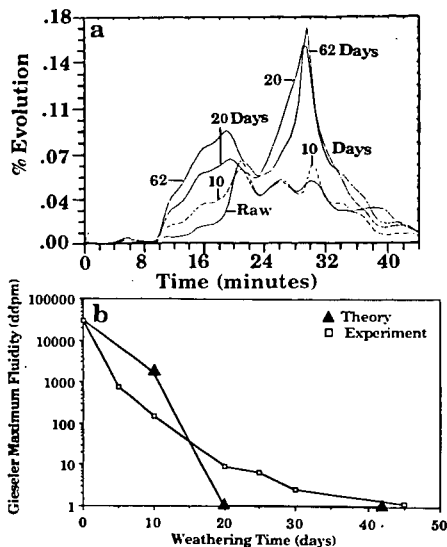


Figure 31. Reduction in Fluidity with Weathering: a) CO_2 Evolution of Raw and Weathered Coal, and b) Predicted and Measured Fluidity (Measurements of Wu et al. Ref. 79). Weathered Coal was Kept at 80°C for the Indicated Number of Days.

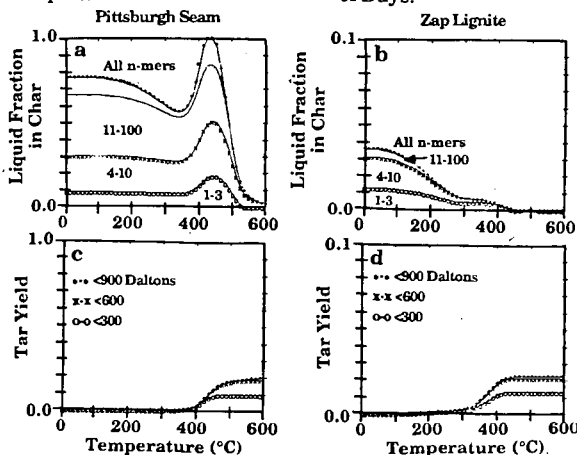


Figure 32. Predicted Molecular Weight Distribution in Char and Tar for a Bituminous Coal and a Lignite. a) and b) Molecular Weight Distribution for Char, and c) and d) Molecular Weight Distribution for Tar.

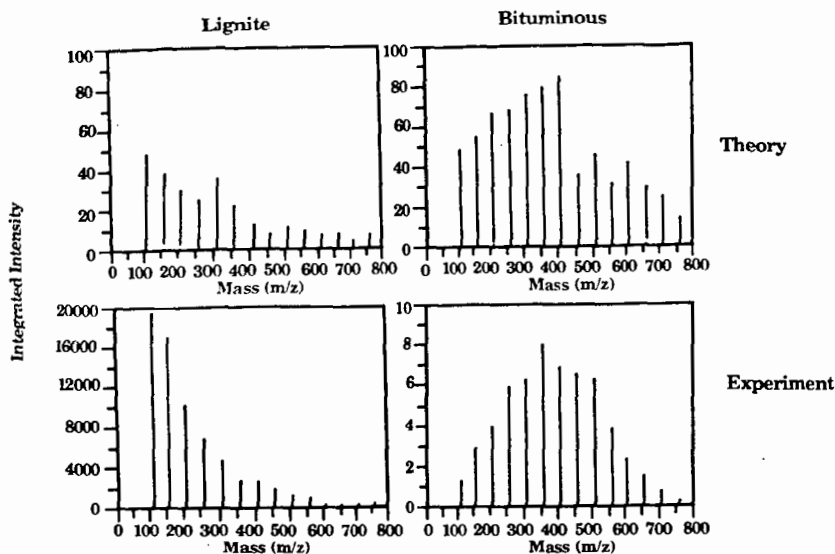


Figure 33. Comparison of Measured and Predicted Tar Molecular Weight Distributions for Lignite and Bituminous Coals. The Experiments are Performed by Pyrolysis of Coal Samples in a FIMS Apparatus. Intensities have been Summed over 50 AMU Intervals.

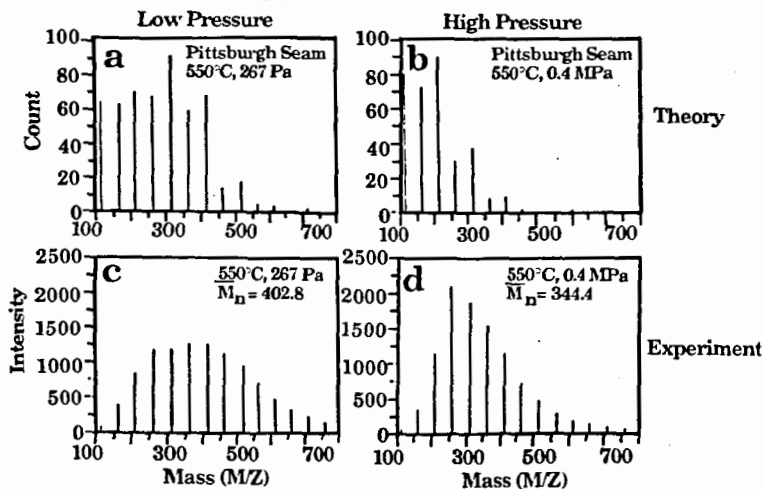


Figure 34. Comparison of Predicted (a and b) and Measured (c and d) Tar Molecular Weight Distribution for Pyrolysis of a Pittsburgh Seam Coal in a Heated-Grid Apparatus at a Heating Rate of 500°C/s to 550°C. Parts a and c Compare the Prediction and the Measurement at 0.00267 atm. Parts b and d Compare the Prediction and Measurement at 4.0 atm. $P = 0.2$ atm.

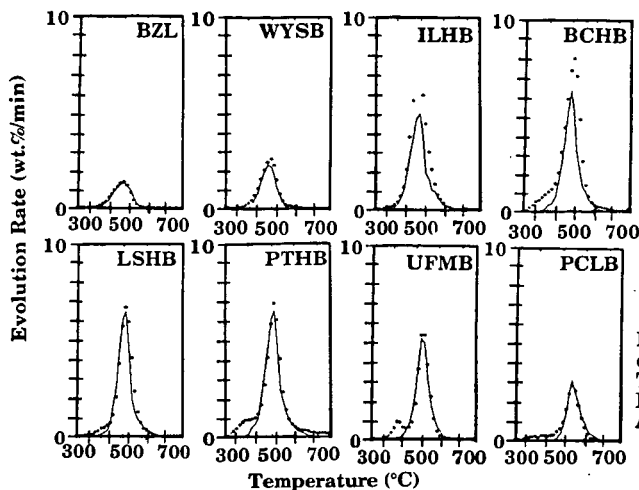


Figure 35. Comparison of Measured and Predicted TG-FTIR Analysis of Tar Evolution for the Eight Argonne Coals.

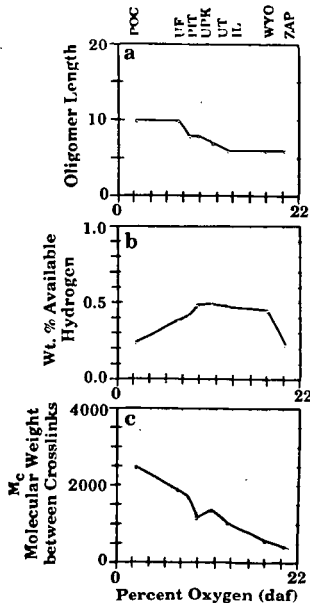


Figure 36. Network Parameters for Monte Carlo Version of FG-DVC Model for Eight Argonne Coals. a) Oligomer Length, b) Weight Percent of Available Hydrogen and c) Molecular Weight Between Crosslinks, M_c .

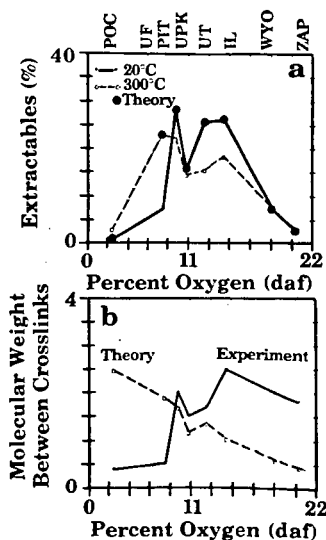


Figure 37. Comparison of Experimental and Theoretical Parameters for a) Extractables and b) Molecular Weight Between Crosslinks.